

**Pre- and Perioperative Assessment of Right Ventricular Afterload to Determine Chronic  
Right Ventricular Failure Post-implant of Durable Left Ventricular Assist Device:  
Feasibility and Clinical System Development**

by

**Timothy Nicholas Bachman**

Bachelor of Science in Engineering, University of Pittsburgh, 2004

Master of Science in Bioengineering, University of Pittsburgh, 2008

Submitted to the Graduate Faculty of the  
Swanson School of Engineering in partial fulfillment  
of the requirements for the degree of  
Doctor of Philosophy

University of Pittsburgh

2021

UNIVERSITY OF PITTSBURGH

SWANSON SCHOOL OF ENGINEERING

This dissertation was presented

by

**Timothy Nicholas Bachman**

It was defended on

December 17, 2020

and approved by

Harvey S. Borovetz, Ph.D., Professor, Department of Bioengineering

Kang Kim, Ph.D., Associate Professor, Department of Bioengineering

Robert L. Kormos, MD, Professor Emeritus, Department of Cardiothoracic Surgery

Richard D. Schaub, Jr., PhD, Adjunct Assistant Professor, Department of Bioengineering

Dissertation Director: Marc A. Simon, MD, MS, Associate Professor, Department of Medicine  
and Department of Bioengineering

Copyright © by Timothy Nicholas Bachman

2021

**Pre- and Perioperative Assessment of Right Ventricular Afterload to Determine Chronic Right Ventricular Failure Post-implant of Durable Left Ventricular Assist Device: Feasibility and Clinical System Development**

Timothy Nicholas Bachman, PhD

University of Pittsburgh, 2021

Patients suffering from end-stage heart failure refractory to optimal medical treatment may require a durable left ventricular assist device (LVAD) as a bridge to transplant or as destination therapy. Unfortunately, as many as 40% of LVAD recipients experience right ventricular failure (RVF) post-implant. RVF post-implant results in a decrease in survival to transplant or continued support, and an increase in hospital stay. In the most severe RVF cases, mechanical circulatory support (MCS) for the right ventricle (RV) is needed. Short-term RV MCS is available; however, no durable RVAD currently exists. To date, research has focused mainly on predicting cases of RVF which occur immediately following LVAD implant or within the first 30 post-operative days. However, chronic RVF may also occur in subjects beyond one month.

In the clinical setting, echocardiography (echo) and right heart catheterization (RHC) are standard methods used to provide imaging and hemodynamic data for physicians. RHC reports resistance faced by the RV using only mean pressure and mean flow. However, it does not account for the oscillatory component of pulsatile blood flow generated during the cardiac cycle. Pulmonary vascular impedance (PVZ) completely characterizes the RV afterload by measuring both steady and oscillatory components in the frequency domain. Unfortunately, PVZ has not been used in the clinical setting due to technical limitations and cost-prohibitive equipment.

In this study, we attempted to calculate PVZ using signals obtained via standard of care echo and RHC, available before and during LVAD implantation. PVZ spectra were then used to

determine if there is a difference in RV afterload based on RVF outcome within one year of implant. Results ultimately showed that there was no difference in afterload between groups.

Though no difference in PVZ was found, the study showed that PVZ calculation is possible and may be of benefit to other patients. Following completion of the initial study, a graphically driven, software-based system was developed to calculate PVZ using only standard of care data from electronic health records. The software facilitates rapid assessment of PVZ in a manner that is intuitive to those who work in the clinical setting.

# Table of Contents

<b>Preface.....</b>	<b>xvii</b>
<b>1.0 Introduction.....</b>	<b>1</b>
<b>1.1 Normal Cardiac Function.....</b>	<b>1</b>
<b>1.1.1 Cardiac Anatomy and the Cardiac Cycle .....</b>	<b>1</b>
<b>1.1.2 Preload, Afterload, and stroke volume .....</b>	<b>3</b>
<b>1.2 Heart Failure.....</b>	<b>5</b>
<b>1.3 Standard of Care Hemodynamic Assessment.....</b>	<b>6</b>
<b>1.3.1 Echocardiography and Pulsed-wave Doppler Velocity .....</b>	<b>7</b>
<b>1.3.2 Right Heart Catheterization .....</b>	<b>8</b>
<b>1.4 Pulmonary Vascular Impedance.....</b>	<b>11</b>
<b>1.5 Left Ventricular Assist Devices .....</b>	<b>13</b>
<b>1.5.1 Current Designs.....</b>	<b>14</b>
<b>1.5.2 Categorizing LVAD Candidates .....</b>	<b>16</b>
<b>1.5.3 Surgical Implantation .....</b>	<b>17</b>
<b>1.5.4 LVAD Physiology .....</b>	<b>18</b>
<b>1.5.5 Right Ventricular Failure post-LVAD Implantation .....</b>	<b>20</b>
<b>2.0 Hemodynamic Assessment of Pre- and Perioperative Afterload as an indicator of Chronic RV Failure post-LVAD Implant.....</b>	<b>24</b>
<b>2.1 Ethical Considerations .....</b>	<b>24</b>
<b>2.2 Data Acquisition and Timeline.....</b>	<b>25</b>
<b>2.3 Assessment of RV Afterload in the Time Domain.....</b>	<b>31</b>

<b>2.3.1 Description .....</b>	<b>31</b>
<b>2.3.2 Methods.....</b>	<b>31</b>
<b>2.3.3 Statistical Methods.....</b>	<b>32</b>
<b>2.3.4 Results .....</b>	<b>32</b>
<b>2.4 Assessment of RV Afterload in the Frequency Domain using Pulmonary Vascular Impedance .....</b>	<b>38</b>
<b>2.4.1 Description .....</b>	<b>38</b>
<b>2.4.2 Methods.....</b>	<b>38</b>
<b>2.4.3 Statistical Methods.....</b>	<b>38</b>
<b>2.4.4 Results .....</b>	<b>39</b>
<b>2.5 Discussion .....</b>	<b>45</b>
<b>3.0 Facilitation of Rapid Assessment of Pulmonary Vascular Impedance in the Clinical Setting .....</b>	<b>47</b>
<b>3.1 Description .....</b>	<b>47</b>
<b>3.2 Methods .....</b>	<b>48</b>
<b>3.3 Results.....</b>	<b>54</b>
<b>3.4 Discussion .....</b>	<b>56</b>
<b>4.0 Conclusions and Future Directions .....</b>	<b>57</b>
<b>Appendix A.....</b>	<b>60</b>
<b>Bibliography .....</b>	<b>67</b>

## List of Tables

<b>Table 1- Patient Cohort .....</b>	<b>29</b>
--------------------------------------	-----------

## List of Figures

- Figure 1- Diagram of blood flow, basic cardiac anatomy, and major vessels. Solid blue indicates de-oxygenated blood; solid red indicates oxygenated blood; dark maroon indicates myocardium and valves. (Left) Long axis view of heart with arrows indicating normal direction of blood flow in heart and great vessels. (Right) Short axis view of ventricles illustrating thin-walled crescent shape of right ventricle, attached to circular left ventricle plus septum with thick walls..... 3**
- Figure 2- Dilation of the ventricles during ventricular failure. (Left) Long axis and short axis diagram of a normal heart. (Right) Long axis and short axis diagrams of dilation cause by left ventricular failure and reduced cardiac output. Thickness of white arrows indicate proportional differences in flow..... 6**
- Figure 3- Pulsed-wave Doppler velocity of pulmonary artery. The two-dimensional image sector at the top of the image shows the location where the pulsed-wave doppler velocity is being measured. The periodic signal is the doppler signal converted to velocity. The electrocardiogram of the heart is superimposed at the bottom of the image..... 8**
- Figure 4- (Top) Swann-Ganz catheter with balloon tip inflated. (Left) Diagram of path taken by Swann-Ganz catheter (green) when introduced via jugular vein, through the superior vena cava, into the right atrium (RA), then right ventricle (RV), and eventually into the pulmonary artery (PA). When advanced into smaller vessels followed by inflation of the balloon tip, the back pressure from the left atrium, referred to as the pulmonary capillary wedge pressure (PCWP) can be measured. (Right) Pressure waveforms obtained during**

right heart catheterization in each region as the catheter proceeds forward in the same direction as blood flow..... 10

**Figure 5- Visual depiction of calculating pulmonary vascular impedance (PVZ) and the resulting spectrum. (Top left) Pulmonary arterial pressure and pulmonary arterial flow are recorded in the time domain. (Bottom left) Waveforms are decomposed into wavelets and described in the frequency domain via Fast Fourier Transform (FFT) starting at the fundamental frequency  $z(1)$ , (first harmonic, which is inverse of heart rate) and subsequent multiples of the first harmonic. (Top right) PVZ is calculated as the ratio of flow to pressure in the frequency domain. (Bottom right) Results of the modulus of PVZ are displayed visually as a 2D plot of  $PVZ(z)$  vs  $z$ ..... 12**

**Figure 6- Image reconstructions from CT scans of patients with left ventricular assist devices (LVADs) connected to apex of left ventricle and ascending aorta. (Left) First generation HeartMate XVE pulsatile LVAD, which contained a large pusher plate and valves to ensure unidirectional flow. (Right) Second generation HeartMate II, a valveless continuous flow LVAD which required a much smaller surgical pocket for implantation and could be used on smaller patients. Adapted from reference number [13]. ..... 14**

**Figure 7- The three durable left ventricular assist device (LVAD) models encountered in this work. (Left) the 2<sup>nd</sup> generation HeartMate II axial flow LVAD with mechanical bearing, (middle)the third generation HeartWare HVAD centrifugal flow LVAD with a hydrodynamic thrust bearing, and (Right) third generation HeartMate 3 centrifugal flow LVAD which is fully magnetically levitated. .... 16**

**Figure 8- Normal direction of blood flow in setting of left ventricular assist device at full support, and the resultant unloading of the LV. LVAD = left ventricular assist device.. 19**

**Figure 9- Example of how an “H-Q Curve” may look like for a specific continuous flow LVAD. A change in speed or in pressure may increase or decrease the resulting pump flow. Depending on the pump design, the curves may be steeper or flatter based on sensitivity to afterload.  $\Delta P$  = Pressure drop across the pump (the difference of afterload minus preload), L/min = liters/ min. .... 20**

**Figure 10- Direction of blood flow in setting of RV Failure post-LVAD implant. Altered geometry of RV and LV due to overload of the RV and unloading of LV can cause septal shift, resulting in RV dysfunction. Thickness of white arrows are proportional to flow. RV = right ventricle; LVAD = left ventricular assist device. .... 23**

**Figure 11- Study Timeline describing how data were obtained, location, status, level of LVAD support, and data sources available at each timepoint. The red arrow indicates progression of time, and the blue arrow indicates timepoint at which LVAD support has started (T(3))..... 26**

**Figure 12- Examples of traced signals that were obtained during the perioperative period. (Top Left) Parasternal short axis view taken at base of the heart during a transesophageal echo, and measurement of pulmonary artery diameter. (Top Right) Tracing of Pulsed-wave Doppler signal and ECG signal obtained during transesophageal echo. (Bottom) Tracing of pulmonary arterial pressure signal obtained from Swann-Ganz catheter in operating room, and ECG signal..... 28**

**Figure 13-Quarterly count of studies where data were acquired, color coded by device. Early in the study, implants where data were acquired were comprised mainly of HeartWare and HeartMate II devices. However, towards the second half of the study, Heartmate 3’s were encountered more frequently. Qtr = quarter ..... 30**

**Figure 14-(Top) Visual representation of pressure data acquired per patient by stage. (Bottom) pressure data acquired per patient by outcome. Abbreviations: (-)RVF = no RV failure, (+)RVF = RV Failure, TX = transplant before one year, DEC = deceased before one year, EXC = excluded from study per surgeon request. Although only 51 subjects were included in the cohort, 52 studies were observed. At the request of the surgeon a subject was excluded from the study..... 34**

**Figure 15- (Left) Average representative beats (ARBs) for each timepoint. (Right) Parameters derived by from each ARB at each timepoint. (Bottom) Conditions for each timepoint. (Abbreviations: PA= Pulmonary Artery, PAP = PA pressure (mmHg), s = systolic, d = diastolic, m = mean, HR= heart rate (beats/min), MAP = Mean Aortic Pressure (systemic, mmHg), RAP = right atrial pressure (mmHg), CVP= central venous pressure (mmHg), PCWP = pulmonary capillary wedge pressure (mmHg), PAPI = PA pulsatility index. .... 35**

**Figure 16- Pressure-derived parameters in the time domain versus timepoint (T) for subjects with RVF (Red) and without RVF (Blue). Vertical line at T(3) indicates timepoint of LVAD implant. (Abbreviations: RVF = right ventricular failure; PA= Pulmonary Artery, PAP = PA pressure (mmHg), sys = systolic, dia = diastolic, m = mean, MAP = Mean Aortic Pressure (systemic, mmHg), RAP = right atrial pressure (mmHg), CVP= central venous pressure (mmHg), PCWP = pulmonary capillary wedge pressure (mmHg), PAPI = PA pulsatility index. .... 36**

**Figure 17- Count of PA Doppler signals by stage and by outcome. These waveforms, compined with pressure waveforms from previous section were used to calculat PVZ. Abbreviations: (-)RVF = no RV failure, (+)RVF = RV Failure, TX = transplant before one**

year, DEC = deceased before one year, EXC = excluded from study per surgeon request. Although only 51 subjects were included in the cohort, 52 studies were observed. At the request of the surgeon a subject was excluded from the study..... 40

**Figure 18- Components used for calculation of pulmonary vascular impedance (PVZ) and the resulting spectra from a single subject at all three timepoints. (Top left) Average representative beats for pressure. (Bottom left) Average representative beats for pulsed-wave Doppler velocity. (Top right) Modulus of the impedance spectrum. (Bottom right) Phase difference at each harmonic. Abbreviations: mmHg = millimeters of mercury, mod= modulus, L/min = liters per minute, sec = seconds, cm/s = centimeters/second, rads = radians..... 41**

**Figure 19- Heart rate comparisons for PVZ at all 3 timepoints. One subject at T(2) had an arrhythmia which caused the largest individual difference in heart rate. As a group, T(1) had the heart rate differences, likely due to time elapsed between captures of Doppler Velocity and RHC. Abbreviations: HR = heart rate; RHC = right heart catheterization. .... 42**

**Figure 20-Shortest time to surgery for T(1) vs time between procedures (echocardiography and right heart catheterization for T(1)). Large periods of time may have elapsed between subjects' echo and right heart catheterization, or between last study and implant. Comparison of PVZ by 1-year outcome was later limited to a maximum of 96 hours between captures , and 96 hours between last capture and surgery in order to decrease likelihood of error. PVZ = pulmonary vascular impedance, RHC = right heart catheterization..... 43**

**Figure 21- PVZ spectra and calculated parameter results for subjects with and without RVF (red, and blue, respectively). Dotted line indicates timepoint of device implant. A significant difference could only be found at T(1) for PVS when using the full set of subjects. However, once data were limited to captures that had a time difference of less than 96 hrs (see Figure 20), both between captures and from latest capture to surgery, the data were no longer significant. Abbreviations: RVF = right ventricular failure. PVZ(z) = pulmonary vascular impedance versus harmonic (z), ZS = stiffness, ZC = characteristic impedance, Z0 = total pulmonary resistance (steady component), CI = confidence interval. .... 44**

**Figure 22- Parasternal short axis view of the heart using 2-dimensionall ultrasound. Two measurements are made: The measurement on the left is for calibration purposes, and the measurement on the right is measuring the diameter of the pulmonary artery. .... 50**

**Figure 23- (Top) Automated border detection of pulmonary arterial pulsed-wave Doppler velocity with electrocardiogram. Interference in the signal overlay can be observed at the end of the ECG signal. (Bottom) automated border detection from pulmonary arterial pressure waveform obtained via fluid-filled Swann Ganz catheter and electrocardiogram. .... 51**

**Figure 24- Tracings of Doppler velocity and pressure waveforms separated into individual beats via R-wave detection. .... 52**

**Figure 25- (Left) selection of individual beats for generation of average representative beats (middle). The average representative beats decomposed into wavelets via Fast Fourier Transform to calculate Magnitude (Top Right) and phase (bottom) of pulmonary vascular impedance. .... 53**

**Figure 26- (Top Left) Multiple impedance spectra can be calculated and overlaid from the same capture to show changes due to beat selection. Additionally, spectra can be calculated for multiple timepoints to observe changes during a protocol. (Bottom Left) The end user has the ability to select which spectra to keep and which to hide by checking the “Include” boxes for spectra of choice. (Right) Time series for the resulting parameters from both time and frequency domain are plotted for the selected spectra..... 55**

**Appendix Figure 1- Step 1: Input subject info and import parasternal short axis view at base of the heart (TTE or TEE). The image is calibrated using the image calibration key (the dots on the sector). Following calibration, the diameter of the PA is measured at the insertion sites of the PA valve leaflets. .... 61**

**Appendix Figure 2- Step2: The screen capture of pressure with ECG is imported. Values the image is calibrated by assigning values to the x-axis, y-axis, and origin. The user drags a boxes around the region containing the pressure waveforms. Automated border detection then traces and re-digitizes the selected signals. .... 62**

**Appendix Figure 3- Step3: The screen capture of PA pulsewave Doppler signal is imported. This can be captured either via TTE or TEE. Values the image is calibrated by assigning values to the x-axis, y-axis, and origin. The user drags a boxes around the region containing the doppler and ECG waveforms. Automated border detection then traces and re-digitizes the selected signals. Due to low signal-to-noise ratio in Doppler signals, the user can make edits to remove any artifacts in Doppler tracing..... 63**

**Appendix Figure 4- Step 4: individual beats are automatically identified using ECG signal to generate an R-R interval. If unsatisfactory, user can repeat steps 2 and/or 3 to improve signal fidelity..... 64**

**Appendix Figure 5- Step 5: User selects pressure and velocity beats to form average representative beats in tie domain and perform FFT to calculate a PVZ spectra. The user has the option of recording notes. Once satisfied with spectra, user saves it to PVZ History for comparison. .... 65**

**Appendix Figure 6- Step 6: The user selectes which PVZ spectra to compare graphically by checking or unchecking boxes in bottom left table. Spectra that are selected remain visble, and paraters derived from spectra are plotted in series on the right. All data (both selected and unselected) are exported in a .csv file once complete. The spreadsheet indicates which spectra were selected and deselected..... 66**

## **Preface**

I would like to use this section to thank everyone who has encouraged me, motivated me, worked with me, or has simply listened to me throughout the years as I worked toward this degree. To my parents, who have always supported my interest in the sciences, I am forever grateful. To the professors, physicians, staff, who encouraged me to pursue a Ph.D., I thank you for the push. To the Vascular Medicine Institute, which allowed me to work towards my goal while still employing me, I thank you for the flexibility. To the students and residents who worked with me, I thank you for your tenacity. To the friends who had to listen to me, I thank you for your patience and positivity. Finally, to the patients that I have helped to care for over the years, I thank you for your inspiration.

## **1.0 Introduction**

The purpose of this work is to describe the pulsatile load encountered by the right ventricles of patients receiving left ventricular assist devices to determine if there is a difference between those who suffer from right ventricular failure post implant, versus those who do not. In addition, this work attempts to create a solution to the hurdles that have previously limited the use of pulmonary vascular impedance in the clinical setting.

This will require a basic understanding of ventricular function, ventricular failure, ventricular assist devices, and the methods used to assess the hemodynamics experienced during implantation. This chapter will briefly cover these topics.

## **1.1 Normal Cardiac Function**

### **1.1.1 Cardiac Anatomy and the Cardiac Cycle**

The heart is a four-chambered muscular organ responsible for pumping blood to the organs throughout the body. The blood delivers oxygen and nutrients to organs in the body while also removing waste and carbon dioxide generated by cells. The heart can be thought of as two pumps in one (left and right), separated by a septal wall, connected in series in a closed loop. As shown in Figure 1, the left side of the heart is responsible for receiving oxygenated blood from the lungs and pumping it to organs such as the brain and kidneys (the systemic circuit), while the right side is responsible receiving de-oxygenated blood returning from end organs, and then pumping it to

the lungs (pulmonary circuit). Each side has two chambers: the atrium and ventricle. The atria assist with filling of the ventricles which are the main pumping chambers of the heart. The right ventricle (RV) and left ventricle (LV) pump blood through the pulmonary and systemic circuits, respectively.

The atria and ventricles are separated by valves that ensure unidirectional flow. Between the left atrium (LA) and LV is the mitral valve, and between the right atrium (RA) and RV is the tricuspid valve. These valves open when the ventricles relax during filling, or diastole, and close when the ventricles contract during ejection, or systole. The valves between the LV and Aorta (AO) and between the RV and Pulmonary artery (PA) are the aortic valve and pulmonic valve, respectively. These valves are closed during diastole, and open during systole. In between systole and diastole, there exists two phases where all valves are closed. They are referred to as isovolumetric contraction and isovolumetric relaxation. The entire process of filling and ejecting is called the cardiac cycle. The frequency of the cardiac cycle is the heart rate (HR). The volume of blood that is ejected per beat is referred to as the stroke volume (SV). The periodic ejection of blood by the ventricles into the PA and AO generates pulsatile blood flow.

Although both ventricles eject blood from the heart, they are very different in shape and wall thickness. The LV is an ellipsoidal shaped muscular chamber. This is due to high vascular resistance generated by the systemic circuit, which the ventricle must overcome to pump blood throughout the body. Typically, the septum is treated as part of the LV, however, it still contributes to RV contraction. The RV is a thin-walled complex crescent shape that attaches to and wraps around the right side of the LV. The RV free wall is less muscular and requires less force to eject blood because it pumps into a low resistance, high compliance pulmonary circuit. This will be discussed further in the next section.

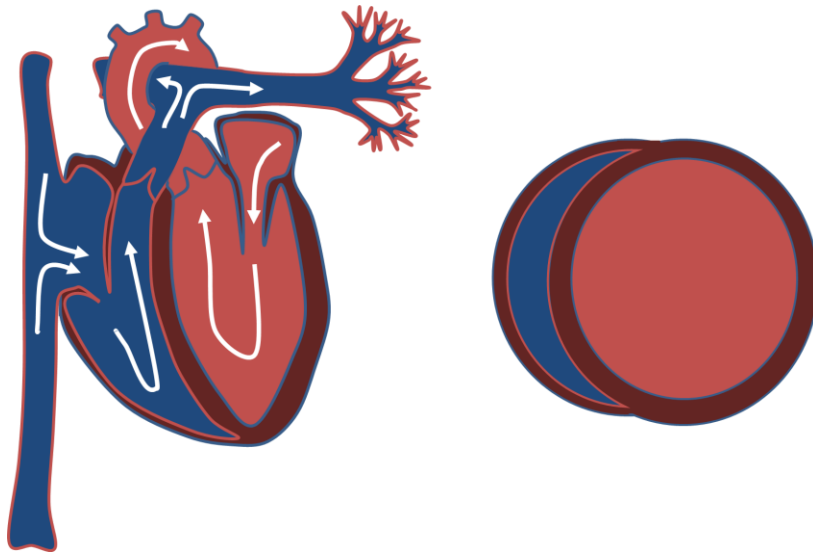


**Figure 1- Diagram of blood flow, basic cardiac anatomy, and major vessels. Solid blue indicates de-oxygenated blood; solid red indicates oxygenated blood; dark maroon indicates myocardium and valves. (Left) Long axis view of heart with arrows indicating normal direction of blood flow in heart and great vessels. (Right) Short axis view of ventricles illustrating thin-walled crescent shape of right ventricle, attached to circular left ventricle plus septum with thick walls**

### **1.1.2 Preload, Afterload, and stroke volume**

The total amount of blood that is ejected per unit time (typically in liters per minute for humans) is referred to as the cardiac output (CO) and is the product of SV x HR. This means that the CO ultimately increases or decreases with changes in heart rate or with stroke volume to meet the body's demands. For instance, CO increases during exercise, and decreases at rest. The normal ventricle typically ejects between 50-70% of the end diastolic volume. This percentage is referred to as the ejection fraction (EF). The SV is determined by the end-diastolic volume (EDV) and resulting end-diastolic pressure (EDP), also known as pre-load. The more the ventricle fills, the

greater the pre-load. Preload affects wall stress ( $\sigma$ ) of either ventricle. When assumed to be a sphere,  $\sigma$  is a product of the pressure (P) and ratio of the radius r divided by twice the wall thickness (h), as per the Law of Laplace. The greater the preload, the greater the wall stress, and the harder the ventricle contracts, which is the basis of the Frank-Starling Law of the Heart. The force generated by the ventricle at a given pre-load is referred to as the contractility. Contractility is controlled by the autonomic nervous system, it can also be increased or decreased by certain medications referred to as positive and negative inotropes, respectively. [1]

The afterload is ultimately what the ventricle is pumping against. It is the source of wall stress during cardiac contraction and influences stroke volume opposite that of pre-load. With an increase in afterload comes a decrease in stroke volume. Afterload is composed mainly of steady resistance, which is the mean pressure divided by mean flow. However, due to the pulsatile flow generated by the heart, there are additional oscillatory components of afterload that the heart encounters, which include inertance of blood, wave reflection and vascular compliance.

Both ventricles encounter afterloads composed of resistance, compliance, inertance, and wave reflection. However, the degree to which RV and LV afterload is influenced by each afterload component differs due to location of the main sources of compliance and wave reflection .[2, 3]

## 1.2 Heart Failure

Heart failure (HF) is the inability to supply adequate blood flow to meet the body's metabolic demand. Heart failure with reduced ejection fraction (HFrEF) comprises approximately 49% of HF cases, while heart failure with preserved ejection fraction (HFpEF) comprises approximately 51% of HF cases.[4] As of 2017 the death rate (age adjusted) with any mention of heart failure was 89.7 per 100,000 in the United States, with a total of 80,480 deaths (36,824 males and 43,656 females). The one-year case fatality rate for HF is 29.7%. The economic impact is significant as well. In 2012, the cost of heart failure was 30.7 billion dollars, and is expected to double by 2030. [5]. (Since HFpEF patients are typically not candidates for MCS, focus will be placed on patients with HFrEF in this document).

The severity of HF is classified by New York Heart Association Functional Class I-IV, with class IV being the most severe.[4] In the early stages of heart failure medical therapy may provide adequate support for patients. However, as dilation continues and EF decreases (Figure 2) wall stress increases as previously described by the Law of Laplace. The myocardial thickness may increase to initially compensate for dilation. Unfortunately, such remodeling will only help for a short time due to increased energy requirements in an already failing ventricle, resulting in further decline. If a patient's HF remains refractory to optimal medical treatment, heart transplantation may need to be considered. Although heart transplantation remains the gold standard for treating end stage heart failure, donor hearts are in limited supply; additionally, some patients may not be candidates for transplant. Therefore, mechanical support may need to be considered. [6]

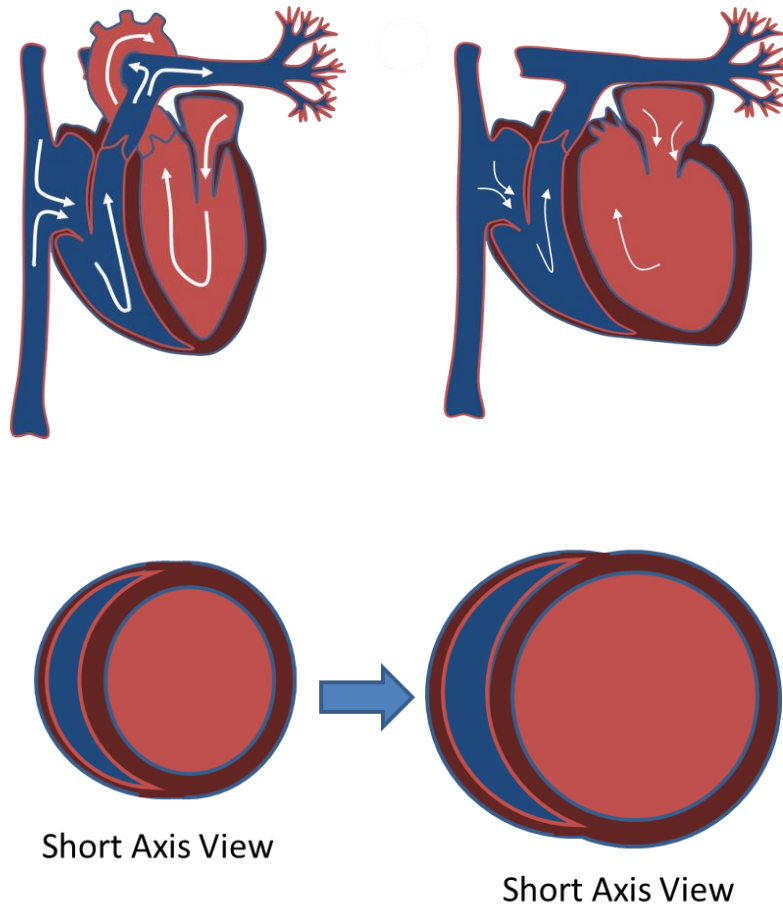


**Figure 2- Dilation of the ventricles during ventricular failure. (Left) Long axis and short axis diagram of a normal heart. (Right) Long axis and short axis diagrams of dilation cause by left ventricular failure and reduced cardiac output. Thickness of white arrows indicate proportional differences in flow.**

### **1.3 Standard of Care Hemodynamic Assessment**

To study how a patient's heart is performing, a mix of imaging and hemodynamic studies must be obtained. Two of the most common means of assessing cardiac function include echocardiography (echo) and right heart catheterization (RHC). There are additional procedures,

such as CT Scans, MRI, and nuclear studies that may be ordered by physicians, however this work will focus echo and RHC. [4]

### **1.3.1 Echocardiography and Pulsed-wave Doppler Velocity**

Echocardiography involves the use of high-frequency ultrasound waves to study the anatomy and function of the heart. The soundwaves are emitted by a probe that is placed on a patient's chest (transthoracic echo, or TTE), or down a patient's esophagus and into the stomach (transesophageal echo, or TEE). [7, 8] The soundwaves that are emitted reflect aback to the probe at a shifted frequency. In 2D Echo, an image of the heart is formed by the difference in the two frequencies and shows wall and valve motion.

During the same procedure, an additional signal is acquired called pulsed wave doppler velocity. Like 2D images, a sound wave is emitted by the same probe. The frequency of the soundwaves either increase if blood flow is moving towards the probe or decrease if they are moving away due to the Doppler Effect. The resulting signal difference produces a spectrogram as shown in Figure 3 . Because the frequency emitted and received is known along with the speed of sound in blood, the velocity of blood flow at a selected location can be measured by tracing the maximal frequency of the spectrogram. If the diameter of the vessel where the signal is measured is known (in this case the PA) the velocity can be multiplied by the cross sectional area ( $\frac{1}{4}$  the diameter squared) to calculate instantaneous flow ( $Q(t)$ ).

Advantages of echocardiography include that it is noninvasive, relatively inexpensive, and therefore widely available. Limitations include conditions which may impair image acquisition, such as obesity and lung disease. Additionally, image quality is dependent upon the sonographer.

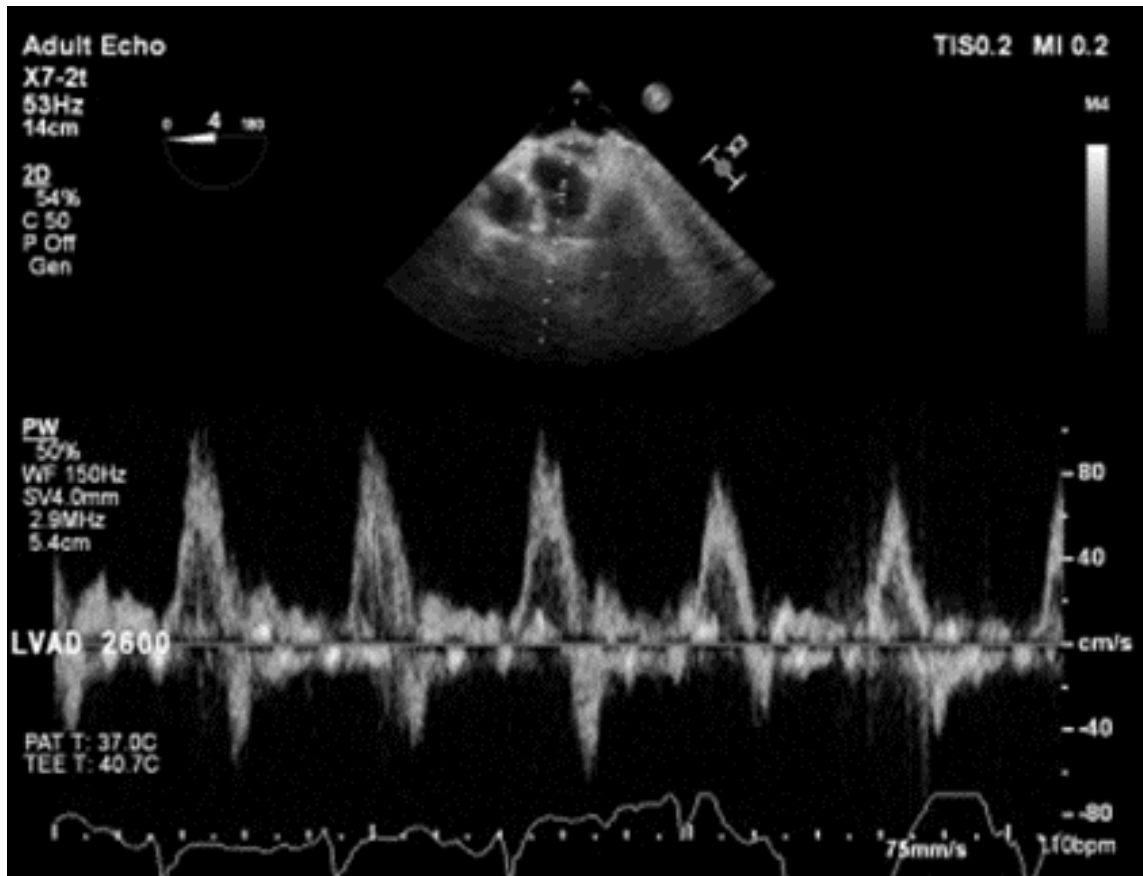


Figure 3- Pulsed-wave Doppler velocity of pulmonary artery. The two-dimensional image sector at the top of the image shows the location where the pulsed-wave doppler velocity is being measured. The periodic signal is the doppler signal converted to velocity. The electrocardiogram of the heart is superimposed at the bottom of the image.

### 1.3.2 Right Heart Catheterization

Right heart catheterization is the most direct method by which pressure and output in the heart can be measured. It is an invasive procedure that requires the insertion of a fluid-filled tube (catheter) into the jugular vein (or alternatively into the femoral vein via the groin), and then introducing it into the heart via the RA. It is then advanced across the tricuspid valve into the RV, and proceeds through the RV outflow tract (RVOT) into the pulmonary arteries. Instantaneous

pressure waveforms are recorded throughout the procedure via a pressure transducer at the other end of the lumen. The catheter is advanced into the smaller branches of pulmonary arteries until a balloon at the tip is inflated. The balloon occludes the vessel and thereby allows measurement of the back pressure, referred to as the pulmonary capillary wedge pressure (PCWP), which estimates the pressure in the LA and at end-diastole in the LV. The catheter, its path, and the waveforms measured in each chamber or vessel are shown in Figure 4. [9]

The fluid-filled Swann-Ganz catheter does have limitations. Its signal is susceptible to motion artifacts, sometimes referred to as “catheter whip”. Air bubbles in the lumen or transducer may dampen the signal. Also, the physical properties of the lumen may either amplify or dampen certain aspects of a pressure signal due to the catheter’s frequency response.

Advances in technology have addressed the shortcomings of fluid filled catheters. High-fidelity micromanometer wires which have a solid-state pressure sensor at the distal end have a higher signal-to-noise ratio than a fluid-filled catheter; these micromanometers are frequently used in research studies. Unfortunately, they are cost-prohibitive for most cases in the clinical realm.

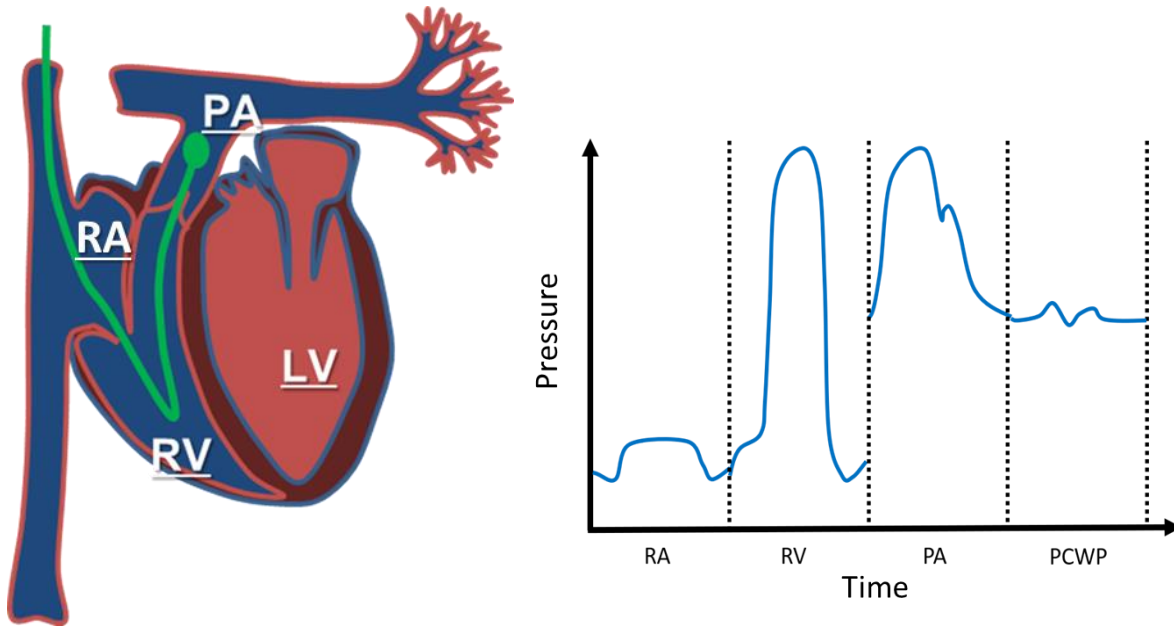


Figure 4- (Top) Swann-Ganz catheter with balloon tip inflated. (Left) Diagram of path taken by Swann-Ganz catheter (green) when introduced via jugular vein, through the superior vena cava, into the right atrium (RA), then right ventricle (RV), and eventually into the pulmonary artery (PA). When advanced into smaller vessels followed by inflation of the balloon tip, the back pressure from the left atrium, referred to as the pulmonary capillary wedge pressure (PCWP) can be measured. (Right) Pressure waveforms obtained during right heart catheterization in each region as the catheter proceeds forward in the same direction as blood flow.

## 1.4 Pulmonary Vascular Impedance

The most comprehensive means by which the RV afterload can be assessed is via pulmonary vascular impedance (PVZ). PVZ was introduced by Milnor et al in the 1960's [10, 11]. It describes both the steady and pulsatile resistance experienced by the RV during ejection. PVZ is not a single value; instead, it must be plotted as a function of values in the frequency domain ( $z$ ). To calculate PVZ( $z$ ), pressure and flow waveforms must be obtained in the time domain. The waveforms are then decomposed via Fast Fourier Transform (FFT) into wavelets at each harmonic. Impedance modulus PVZ( $z$ ) is calculated as the ratio of pressure to flow in the frequency domain. The zeroth harmonic ( $z=0$ , or  $Z_0$ ) is equivalent to mean resistance, or total pulmonary resistance (TPR). The first harmonic ( $Z_1$ ), also referred to as the fundamental frequency, is the inverse of heart rate, and each subsequent harmonic is a multiple of the fundamental frequency (e.g. if HR is 60 bpm, then  $z_1$  is 1 Hz, and  $z_2$  is 2 Hz, and so on). (See Figure 5).

In addition to  $Z_0$ , the first and second harmonic contain a large amount of power and represent the total stiffness (or the inverse of compliance) of the pulmonary vasculature and are influenced by wave reflection. The higher harmonics ( $Z_2$  through  $Z_{10}$ ) represent impedance of the proximal vessels without wave reflection. The mean value of PVZ at higher harmonics is called the characteristic impedance ( $Z_c$ ).

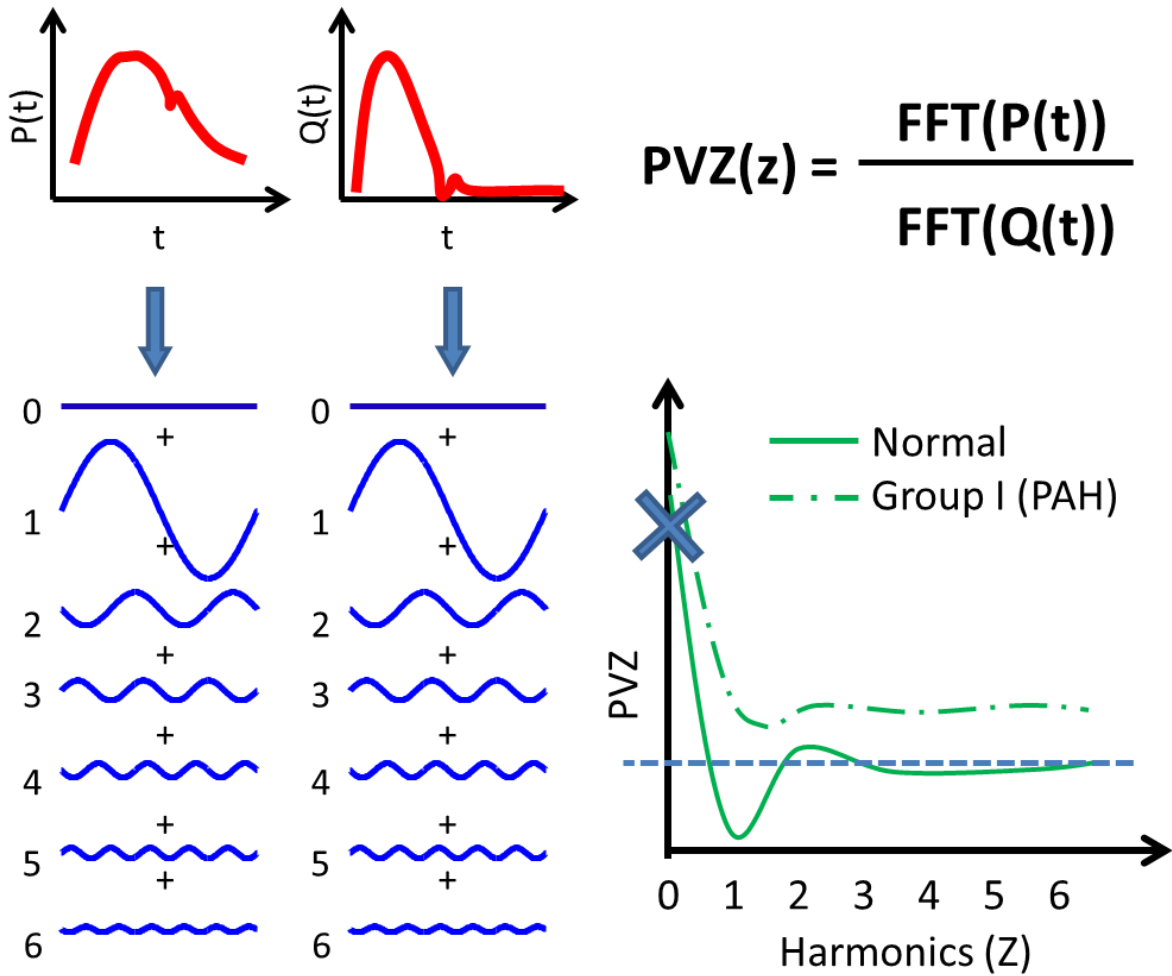


Figure 5- Visual depiction of calculating pulmonary vascular impedance (PVZ) and the resulting spectrum. (Top left) Pulmonary arterial pressure and pulmonary arterial flow are recorded in the time domain. (Bottom left) Waveforms are decomposed into wavelets and described in the frequency domain via Fast Fourier Transform (FFT) starting at the fundamental frequency  $z(1)$ , (first harmonic, which is inverse of heart rate) and subsequent multiples of the first harmonic. (Top right) PVZ is calculated as the ratio of flow to pressure in the frequency domain. (Bottom right) Results of the modulus of PVZ are displayed visually as a 2D plot of PVZ(z) vs z.

## 1.5 Left Ventricular Assist Devices

Left ventricular assist devices (LVADs) are a form of mechanical circulatory support (MCS) that are implanted in a patient suffering from end-stage left ventricular failure. There are multiple forms of mechanical circulatory support devices that are now available to assist LV outside of the operating room, all of which are responsible for unloading the LV and providing adequate perfusion to the systemic circuit. These include temporary devices such as catheter-based intra-aortic balloon pumps (IABPs) and micro-axial pumps, extracorporeal membrane oxygenation (ECMO), and temporary paracorporeal devices. Such temporary devices can only be used for days to weeks before they must be removed, and severely limit a patient's ability to ambulate. There are also long-term left ventricular assist devices that are implanted in patients' chests and provide support for months to years. These "durable" LVADs are the focus of this study and may be referred to as either "LVADs" or "durable LVADs" interchangeably for the remainder of this document.

As shown in Figure 6, an LVAD is connected at the apex of the LV via inflow cannula and the outflow graft is anastomosed to the ascending aorta. The device is powered and controlled by a single transcutaneous driveline that exits the patient's skin at the abdomen and connects to a controller and power source.

The Interagency Registry for Mechanically Assisted Circulatory Support (INTERMACS), which is a registry containing data from 58 sites in the United States that implant FDA approved mechanical MCS devices, reports that from June 2006- December 2018, there have been 24,354 LVADs implanted (this excludes investigational devices). [12]

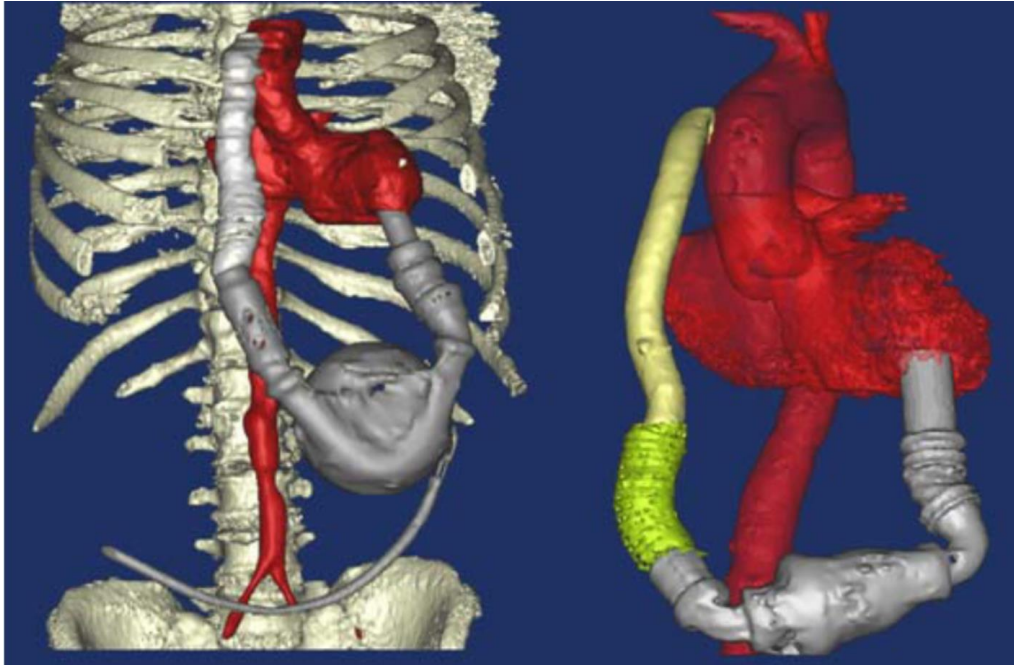


**Figure 6- Image reconstructions from CT scans of patients with left ventricular assist devices (LVADs) connected to apex of left ventricle and ascending aorta. (Left) First generation HeartMate XVE pulsatile LVAD, which contained a large pusher plate and valves to ensure unidirectional flow. (Right) Second generation HeartMate II, a valveless continuous flow LVAD which required a much smaller surgical pocket for implantation and could be used on smaller patients. Adapted from reference number [13].**

### **1.5.1 Current Designs**

First-generation LVAD designs attempted to mimic the pulsatile nature of the native ventricle. Unfortunately, they were too big for all but the largest of patients. Those who did receive an LVAD had to remain connected to large drive systems, had limited mobility, and were required to remain in- or close to the hospital. Originally these devices were only used on patients as a bridge to transplantation. However, it was shown that the same devices could be used even longer periods of time when a transplant was not an option.[14] Still, when an LVAD was originally shown to provide better survival than optimal medical therapy, much improvement was needed in

both areas. LVADs at the time were still too large for many and were susceptible to mechanical failure and thrombus formation.

Continuous flow ventricular assist devices, often referred to as 2<sup>nd</sup> and 3<sup>rd</sup> generation VADs, have replaced the original, larger, pulsatile VADs. The change in design paradigm has significantly decreased the size of VADs, making them available for more patients. For continuous flow VADs, blood is driven by a single moving part, the impellor, which is held in place by a mechanical bearing in the case of 2<sup>nd</sup> generation devices, or in the case of 3<sup>rd</sup> generation devices, by a hydrodynamic thrust bearing or full magnetic levitation. The single moving part increases the longevity of the device, and decreases the likelihood of adverse events such as stroke or mechanical failure. [15] The three main devices implanted at UPMC Presbyterian Hospital during this work were the HeartMate II LVAD (Abbott), HeartWare HVAD (Medtronic), and The HeartMate 3 LVAD (Abbott), which are shown in Figure 7.

The HeartMate II is an axial flow device, where the blood flows along the long axis of the pump. A mechanical bearing holds the impellor in place. The HeartWare and HeartMate 3 devices are centrifugal devices, where the impellor drives blood out at a 90-degree angle from which it enters the device, allowing for a lower profile against the heart when implanted. The impellors for both devices have no mechanical bearing, increasing durability. [16, 17] One drawback of these devices is the non-physiologic flows generated by the impellors. Areas of flow stasis and recirculation can cause thrombus formation. Alternatively, high-speed rotation of the impellor generates areas of higher shear rate which increases chances of hemolysis and may cause platelet activation. In order to mitigate this risk, the impellor blades have been optimized to minimize these regions and to minimize residence time of blood in these regions [18-22]



**Figure 7- The three durable left ventricular assist device (LVAD) models encountered in this work. (Left) the 2<sup>nd</sup> generation HeartMate II axial flow LVAD with mechanical bearing, (middle) the third generation HeartWare HVAD centrifugal flow LVAD with a hydrodynamic thrust bearing, and (Right) third generation HeartMate 3 centrifugal flow LVAD which is fully magnetically levitated.**

**1.5.2 Categorizing LVAD Candidates**

LVADs are intended for patients with dilated NYHA Class IV heart failure refractory to medical therapy, EF < 25%, PCWP > 20, SBP < 80, Cardiac Index < 2 L/min/m<sup>2</sup> and VO<sub>2</sub>max < 14 mg/kg/min. Contraindications include (but are not limited to) hypertrophic cardiomyopathy, severe lung disease, uncorrectable aortic insufficiency, severe independent right heart failure, PVR > 6 WU or transpulmonary gradient (TPG) >15, active bleeding, vascular disease, unresolved stroke, and intolerance to anticoagulation. [23]

INTERMACS has stratified NYHA Class IV further subcategories by clinical status. INTERMACS Class ranges from 1-7, where INTERMACS Class 1 constitutes patients are

experiencing critical cardiogenic shock, Class 2 are patients in progressive decline, Class 3 are stable but inotrope dependent, Class 4 have resting symptoms, Class 5 are exertion intolerant, Class 6 are exertion limited, and group 7 are advanced NYHA Class III. INTERMACS class 2 and 3 are the highest percentage of patients implanted with LVADs.[23, 24]

When selecting patients for LVAD, the course of therapy must also be determined. These are defined in four categories at time of implant but may change later. The first is Bridge to Transplant (BTT), which, as the name states, is the group of patients who require mechanical circulatory support while awaiting transplant. The second category is Destination Therapy (DT) which is intended for patients who are not candidates for transplantation. For some time, those were the only two categories however to more have been added. Bridge to Decision (BTD) patients are those whose categorization as BTT or DT is unknown, and must be re-evaluated after sustained MCS, and Bridge to Recovery patients are those who are likely to experience substantial myocardial recovery while on MCS and may have the LVAD removed without needing a transplant.[12, 23, 25-28]

### **1.5.3 Surgical Implantation**

The surgical process for LVAD implantation involves first placing a patient under general anesthesia. Radial arterial line is placed to monitor arterial pressure along with Swann-Ganz catheter placed via jugular vein to monitor PA pressures throughout the procedure. The anesthesiologist places a TEE probe into the esophagus to assess the heart prior to surgery. This evaluation includes looking for intracardiac shunts, cardiac thrombus, aortic insufficiency, and right ventricular failure.[29]

The surgeon then opens the chest via full sternotomy, followed by tunneling the percutaneous lead. The patient is then placed on cardiopulmonary bypass using arterial and venous cannulation. The apex of the LV is found and cored by the surgeon, who also inspects for any possible thrombus or anatomic obstructions. The LVAD inflow cannula is placed in the apical core with the inlet directed towards the mitral valve. The LVAD is sutured to an apical cuff to secure it in place. The outflow graft is anastomosed to the ascending aorta as it is being de-aired and is then clamped. The heart and pump are then also de-aired. The LVAD is turned on and brought to a low-speed setting until de-airing has been completed. CPB is slowly weaned as pump speed is increased until full LVAD support is reached. The anesthesiologist then evaluates the heart again, looking for air, obstruction, cannula malposition, aortic insufficiency, and RV dysfunction.[29] Speed settings are based on the TEE, arterial pressure, CVP, and PA pressure signals. Finally, the TEE probe is removed, the chest is closed, and the patient is taken to the ICU and [30-32]

#### **1.5.4 LVAD Physiology**

Modern durable LVADs generate continuous flow. During normal operation they provide total- or near-total support of the LV; almost no blood is ejected across the aortic valve, meaning the LV is completely unloaded (Figure 8). Some LVADs are designed to have periodic speed changes to help prevent thrombus formation near the aortic valve and pump. In addition to speed modulation, there remains some native LV function, and thus there may be some fluctuation in flow albeit extremely dampened.[21, 33].

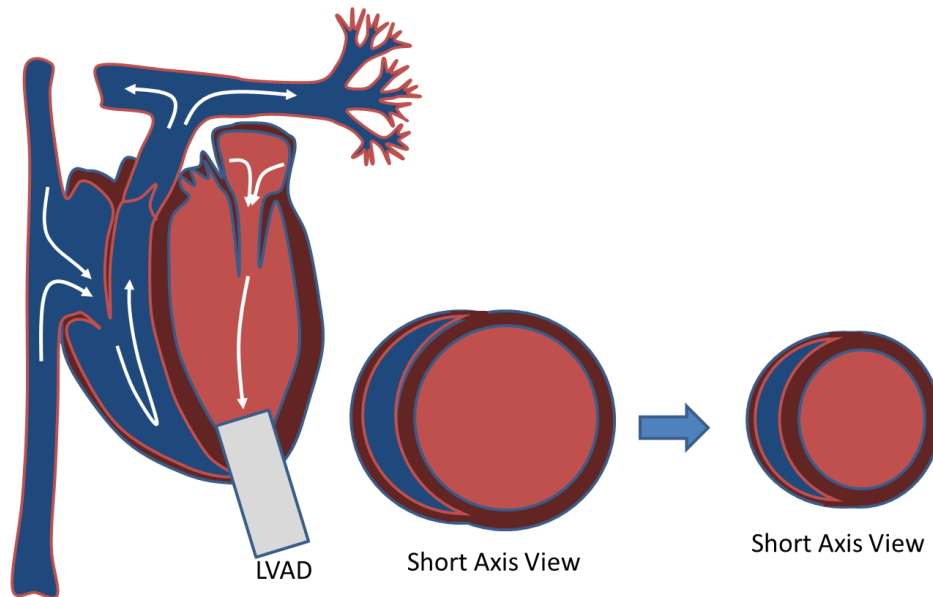


**Figure 8- Normal direction of blood flow in setting of left ventricular assist device at full support, and the resultant unloading of the LV. LVAD = left ventricular assist device.**

The amount of flow generated by the continuous flow LVAD is not only a function of speed, but also a function of preload and afterload. This relationship of speed, pressure difference across the valve and resulting flow is illustrated by an “H-Q” curve resembling the diagram shown in Figure 9. The “Q” stands for flow, and the “H” stands for pressure head, or rather the difference between afterload minus preload ( $\Delta P$ ) across the LVAD. For instance, if a patient is hypertensive, or dehydrated, afterload increases, or preload decreases, respectively. This will increase  $\Delta P$  that the pump must face and result in reduced flow. The opposite also holds true: if, for instance, a patient is volume overloaded, preload increases,  $\Delta P$  decreases, and resulting flow increases. Different pump designs have different sensitivities to preload and afterload. The steepness of the curves, and the changes due to pump speed act as a fingerprint for the device.

The objective of determining the proper pump setting is to balance the desired pump output while not overdriving the pump, creating suction[34, 35] , and/or overloading the RV, which does not have mechanical support and may have previously unknown dysfunction. If suction occurs,

or RV failure occurs, the LVAD output will drop, the LV will not remain unloaded, and the patient may once again begin to experience heart failure symptoms.

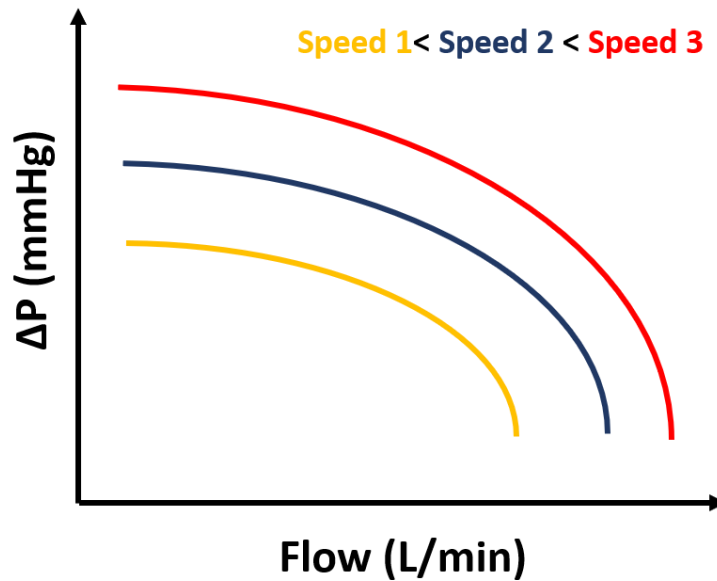


Figure 9- Example of how an “H-Q Curve” may look like for a specific continuous flow LVAD. A change in speed or in pressure may increase or decrease the resulting pump flow. Depending on the pump design, the curves may be steeper or flatter based on sensitivity to afterload.  $\Delta P$  = Pressure drop across the pump (the difference of afterload minus preload), L/min = liters/ min.

### 1.5.5 Right Ventricular Failure post-LVAD Implantation

RV failure post-LVAD implant has been a complication faced by patients since first-generation LVADs have been in use [36]. To date, there remains a great need to improve the ability to predict and monitor RV dysfunction as well as gauge response to treatment to improve overall outcomes with LVAD support.

Kormos et al previously reported that the one-year survival of patients who have received a HeartMate II LVAD as bridge to transplant with early RVF is nearly 20% less than that of

patients with the same device who do not have RVF [37]. Results vary for incidences of RVF post-LVAD in the literature, mainly due to differences in its definition, however it has been reported to range from 9% to 40% as summarized by Patlolla et al. [38] However, it is known RVF results in a decrease in survival to transplant or continued support, and an increase in hospital stay. In the most severe RVF cases, MCS for the RV is needed. Short-term RV MCS is available; however, no durable RVAD currently exists.[39]

RV Failure can occur either early (acute) or late after implant (chronic). Much work has been done to study the former, including novel indices, risk scores and decision support systems; studies of chronic RV failure are less common.[37, 40-50] Even when RV function is normal prior to LVAD implantation, surgical events and the altered physiology of mechanical support may result in RVF. The sudden increase in output from an LVAD and resulting demand placed on the right heart can bring about signs of RV failure that go unnoticed when venous return was minimal prior to implant. RV dysfunction due to LVAD implantation can also occur due to septal shift caused by unloading of the LV (see Figure 10), resulting in increased RV compliance, and decreased RV contractility.[36] Additionally, in some patients, elevated pulmonary vascular resistance (PVR) may persist, even after the pulmonary capillary wedge pressure has decreased due to unloading by the LVAD [51].

RV function is difficult to assess, due in part to its complex crescent-shaped geometry and its interactions with the left ventricle and septum. Comprehensive assessment of RV function, afterload, and coupling are necessary for characterization of the pulmonary circuit. This requires both imaging and invasive hemodynamic assessment.[52]

Conventional transthoracic echocardiography (TTE) and transesophageal echocardiography (TEE) are common techniques use to assess RV function, and right heart

catheterization is performed to assess pressures and cardiac output. What has yet to be done is the full investigation of the RV afterload in the frequency domain, using pulmonary vascular impedance, to determine if there is a difference between patients who experience RV failure (RVF).

Using only the standard of care procedures described in the previous sections, it is the intention of this study to develop a method of analyzing PVZ for LVAD recipients during the pre- and perioperative phase of LVAD implantation. The goal is to determine if there are differences in PVZ between patients who suffer from chronic RV Failure post implant and those who do not. In addition, a system will be developed to make assessment of PVZ more accessible to clinical investigators.

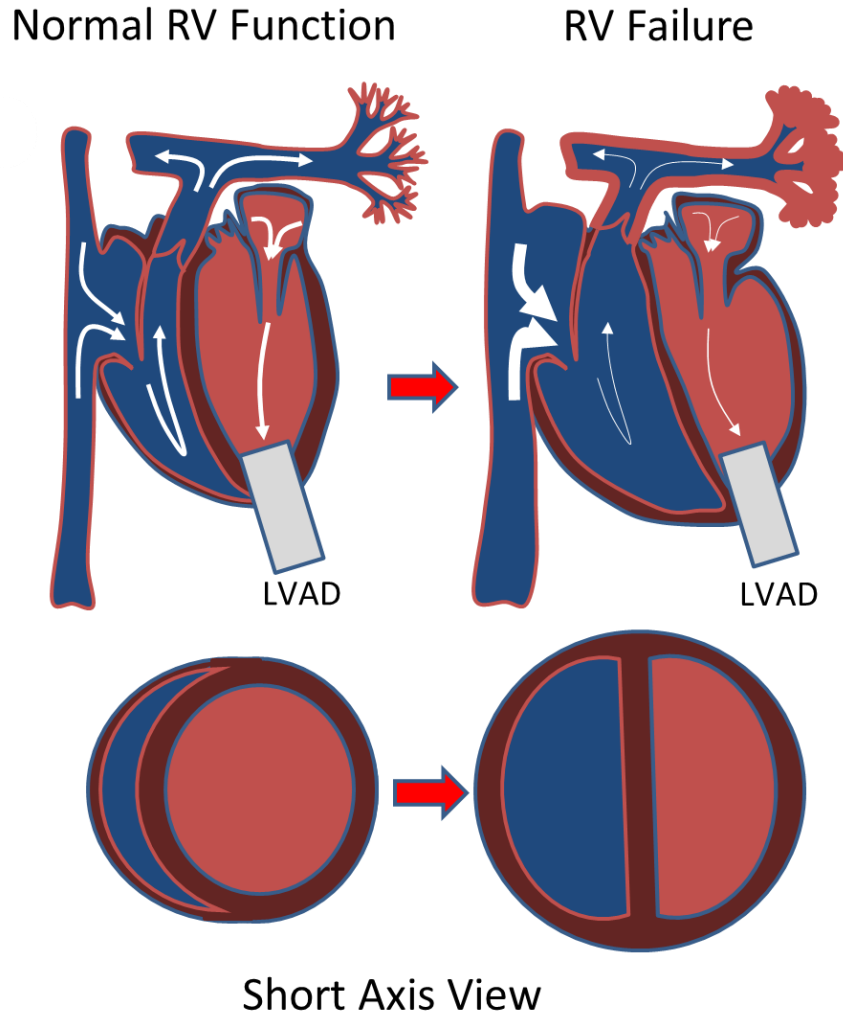


**Figure 10- Direction of blood flow in setting of RV Failure post-LVAD implant. Altered geometry of RV and LV due to overload of the RV and unloading of LV can cause septal shift, resulting in RV dysfunction. Thickness of white arrows are proportional to flow. RV = right ventricle; LVAD = left ventricular assist device.**

## **2.0 Hemodynamic Assessment of Pre- and Perioperative Afterload as an indicator of Chronic RV Failure post-LVAD Implant**

As stated in Chapter 1, PVZ is the most effective way to describe the entire RV afterload. It also has not been used in the clinical setting due to technical, logistical, and financial challenges. This study sought to determine whether there was a difference in the RV afterload of LVAD patients who experience RV failure post implant. We attempted to do so using standard of care hemodynamic studies via right heart catheterization to evaluate afterload in the time domain, and then combined the waveforms with pulsed-wave doppler velocities obtained via TTE and TEE to generate a composite PVZ to characterize the oscillatory and steady components of RV afterload in the frequency domain. We did so at multiple timepoints leading up to and during LVAD implantations to evaluate afterload at different hemodynamic states that are known to occur. The following chapter discusses these studies in detail.

### **2.1 Ethical Considerations**

Prior to LVAD evaluation and implant, patients who are LVAD candidates consent to allow data acquired during standard of care to be used for research purposes. Because the data we obtained were already being obtained during standard of care echoes and RHCs, the need for further consent was waived. Confirmation from the University of Pittsburgh Institutional Review Board was received before proceeding with the study.

## 2.2 Data Acquisition and Timeline

Starting in 2016, pulmonary arterial pressure (PAP) waveforms and/or PA Pulsed Wave Doppler (PW Doppler, or just Doppler) velocity (and ultimately flow (PAQ)) waveforms were captured during standard of care procedures performed during the pre-, peri-, and acute post-operative timepoints of patients who received durable LVAD support. The data were used to calculate hemodynamic measures of RV afterload in both the time and frequency domains. Each timepoint corresponds to a known change in state of the patient which may affect afterload, and thus provide further insight into potential for RV failure.

As illustrated in Figure 11, both pressure and flow data were acquired at three separate time points (T) for this study: Data from T(1) was retrospectively obtained from hemodynamic and echocardiographic studies performed separately while subjects were evaluated for possible durable LVAD support. Data from T(2) and T(3) were both acquired prospectively in the operating room with patients anesthetized; either pre-sternotomy or with chest open, off-bypass and on full LVAD support, respectively. Pressure-only data were acquired for an additional two time points: T(4) immediately following chest closure in the OR, and T(5) within 4-24 hours of chest closure with patient in the intensive care unit (ICU). No PW Doppler velocities were obtained at T(4) and T(5) because it is standard practice to remove the TEE probe prior to chest closure and transport to the ICU.

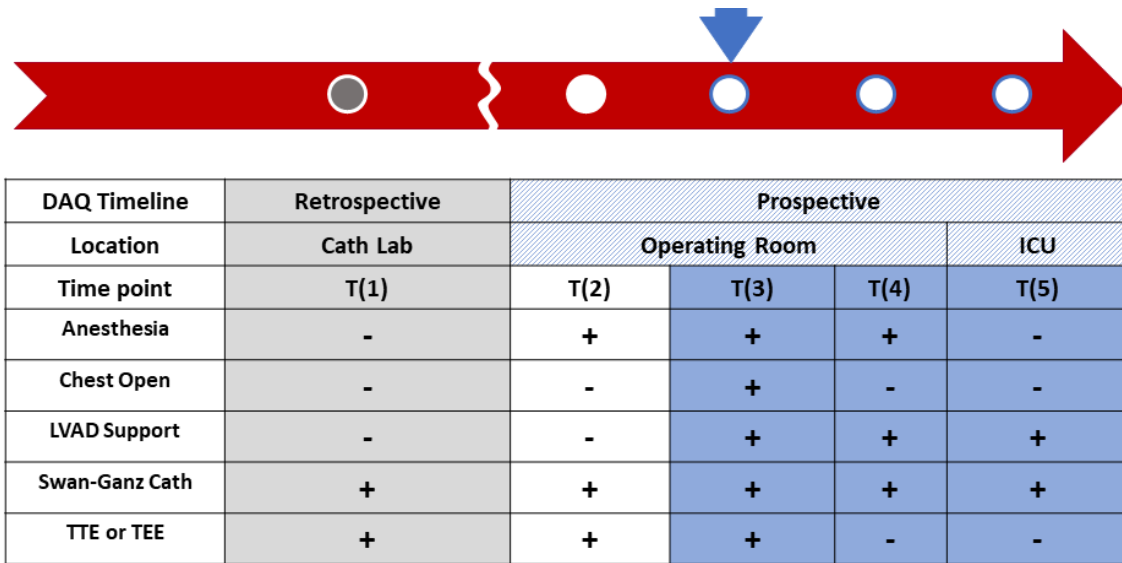


**Figure 11- Study Timeline** describing how data were obtained, location, status, level of LVAD support, and data sources available at each timepoint. The red arrow indicates progression of time, and the blue arrow indicates timepoint at which LVAD support has started (T(3)).

This study included patients who were over the age of 18 and evaluated for durable LVAD as bridge to transplant (BTT) or destination therapy (DT). Patients with prior LVAD (device replacement), temporary RVAD support or ECMO support prior to surgery were excluded from this study. Patients were censored from the study if, before POD 365 sans RVF, death or cardiac transplant occurred. RV failure was determined by chart review of ICD 10 codes and expert adjudication of patient records using INTERMACs definitions at the time.[53]

Screen captures of pre-operative pressure waveforms acquired in the catheterization lab via Phillips system (Phillips North America Corporation, Andover, MA, USA) were saved as JPEG or Bitmap images. Pressure waveforms recorded in the OR were captured and sent to a standard printer by a GE Datex Ohmeda Anesthesia system (GE Healthcare, USA). In the ICU, pressure waveforms were also printed by standard printer from the nurse’s station. Paper printouts were then re-scanned by a standard office copier/scanner as PDFs at a resolution of 600DPI and later

converted to JPEG images. TTE and TEE images of both PA PW Doppler velocities and parasternal short axis views of the base of the heart were downloaded as JPEG images from electronic health records.

Signals were re-digitized using previously published custom-written MATLAB software (MathWorks, Natick Mass, USA). [54] Briefly, images were calibrated using a known scale and waypoints were then added to the waveforms at minima, maxima, inflexion points, and regions of changing slope. The waypoints were then used to fit a piecewise spline curve, that would then be resampled at 1kHz. The re-digitized signals could then be exported for further analysis. Figure 12 shows examples of traced screen captures of Doppler echo and right heart catheter signals obtained during surgery.



**Figure 12- Examples of traced signals that were obtained during the perioperative period. (Top Left) Parasternal short axis view taken at base of the heart during a transesophageal echo, and measurement of pulmonary artery diameter. (Top Right) Tracing of Pulsed-wave Doppler signal and ECG signal obtained during transesophageal echo. (Bottom) Tracing of pulmonary arterial pressure signal obtained from Swann-Ganz catheter in operating room, and ECG signal.**

As shown in Table 1, a total of 51 LVAD recipients were included in this cohort (8 female; 27 ischemic) age  $57 \pm 12$  yrs. Within 365 post-op days (POD), 9 subjects experienced RVF with a mean time to diagnosis of  $176 \pm 111$  days, two of whom also required greater than 14 days of post-operative inotropic support. Ultimately, 11 subjects were censored amongst all 51 subjects (6 deceased, 5 Transplant) prior to the 1-year endpoint or experiencing RVF. Figure 13 shows quarterly count of studies attended during the data collection phase of this work and is color coded based on the device implanted. Early in the study, implants where data were acquired were

comprised mainly of HeartWare and HeartMate II devices. However, towards the second half of the study, Heartmate 3's were encountered more frequently.

**Table 1- Patient Cohort**

	<u>Total</u>	<u>No RVF</u>	<u>Chronic RVF</u>
<b>N (n female)</b>	<b>51 (8)</b>	<b>42 (5)</b>	<b>9(3)</b>
<b>Age mean±SD</b>	<b>56±12</b>	<b>56±12</b>	<b>59± 15</b>
<b>Non-ischemic</b>	<b>24</b>	<b>19</b>	<b>5</b>
<b>INTERMACS Class 1</b>	<b>11</b>	<b>9</b>	<b>2</b>
<b>INTERMACS Class 2</b>	<b>12</b>	<b>10</b>	<b>2</b>
<b>INTERMACS Class 3</b>	<b>21</b>	<b>18</b>	<b>3</b>
<b>INTERMACS Class 4</b>	<b>7</b>	<b>5</b>	<b>2</b>
<b>HeartMate II</b>	<b>8</b>	<b>8</b>	<b>0</b>
<b>HeartMate 3</b>	<b>13</b>	<b>12</b>	<b>1</b>
<b>HeartWare HVAD</b>	<b>30</b>	<b>22</b>	<b>8</b>
<b>Post-op Inotropes &gt; 14 days</b>	<b>7</b>	<b>5</b>	<b>2</b>
<b>Time to chronic RVF (days)</b>	<b>-</b>	<b>-</b>	<b>176±111</b>

**RVF = right ventricular failure; N or n =number; SD = standard deviation**

## Studies and device by Year, Quarter

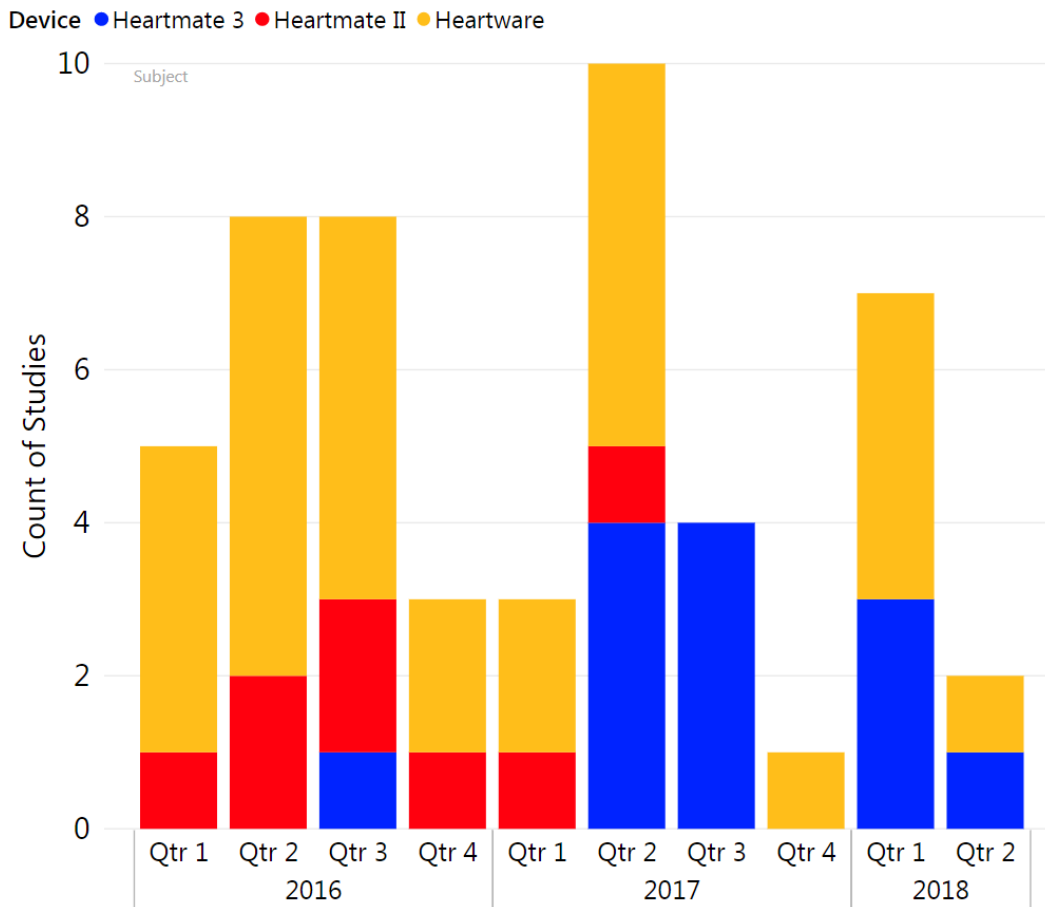


**Figure 13-Quarterly count of studies where data were acquired, color coded by device. Early in the study, implants where data were acquired were comprised mainly of HeartWare and HeartMate II devices. However, towards the second half of the study, Heartmate 3's were encountered more frequently. Qtr = quarter**

## **2.3 Assessment of RV Afterload in the Time Domain**

### **2.3.1 Description**

The initial assessment of patient data involved commonly measured and reported hemodynamic parameters found in the time domain. Therefore, in addition to the waveforms that were redigitized, discrete mean values, on each sheet or in each report, such as central venous pressure, mean aortic pressure, etc. were included in this portion of the study. PCWP was recorded only for T(1), as that was the only timepoint where it was available.

### **2.3.2 Methods**

Redigitized PAP waveforms were imported into custom MATLAB software that allowed selection of multiple, nonsequential beats. An attempt was made to select at least three beats, but fewer were selected if necessary. From the multiple beat selections, an average representative beat (ARB) was calculated at each available timepoint for each subject.

Using the ARBs, the mean, systolic, and diastolic pressures were recorded; heart rate was calculated as the inverse of the cycle period, PA pulse pressure was calculated as the difference between PA systolic and PA diastolic pressures. CVP and RAP were used interchangeably, as was PA diastolic pressure and PCWP. This allowed for an estimation of pulmonary arterial pulsatility index (PAPi), calculated as PA pulse pressure divided by RA pressure, which has been frequently used when studying RVF in the acute and short-term.[55] The ratio of CVP/PCWP, as reported, was also estimated. [39, 56, 57]

### 2.3.3 Statistical Methods

Comparisons between values for subjects with RVF and without RVF at each time point for each parameter were conducted using a Kruskal Wallis H-test. Rate of change for individual parameters between timepoints was also attempted at T(2) to T(3). Finally, a mixed effects mixed effects model was attempted for the rate of change for mPAP and PAPI, as these were determined to be the most likely to have a difference between groups when tested with a pilot set of the data during initial consultation with a biostatistician, and PAPI has shown significance in subjects who experience RVF acute post-op.

### 2.3.4 Results

At least one screen capture of PAP waveforms was obtained for each of the 51 subjects. 39 subjects had recordings at all timepoints. Reasons for 12 subjects missing at least one data point include no pre-op RHC recorded at the institution, catheter malfunction, incorrect positioning, poor signal quality, or early removal prior to 24 hours post chest closure. The composition of the dataset is illustrated in Figure 14, which shows number of captures and outcome for each subject. An example of the of the ARBs and hemodynamic values are shown in Figure 15. (Note that although only 51 subjects were included in the cohort, 52 studies were observed. At the request of the surgeon, this subject was excluded from the study as it was determined that patient required simultaneous pulsatile Bi-VAD support immediately prior to surgery).

Figure 16 shows median and 95% confidence plotted for each hemodynamic parameter, grouped by subjects with RVF and for subjects without RVF at each time point. Minimal separation was found between median values and a wide range for most confidence intervals can

be seen. Differences between standard hemodynamics in the time domain (mPAP, PAPsys, PAPdia, Pulse Pressure, CVP (or RAP)) as well as PAPI were not significant at any T between groups (Figure 5).

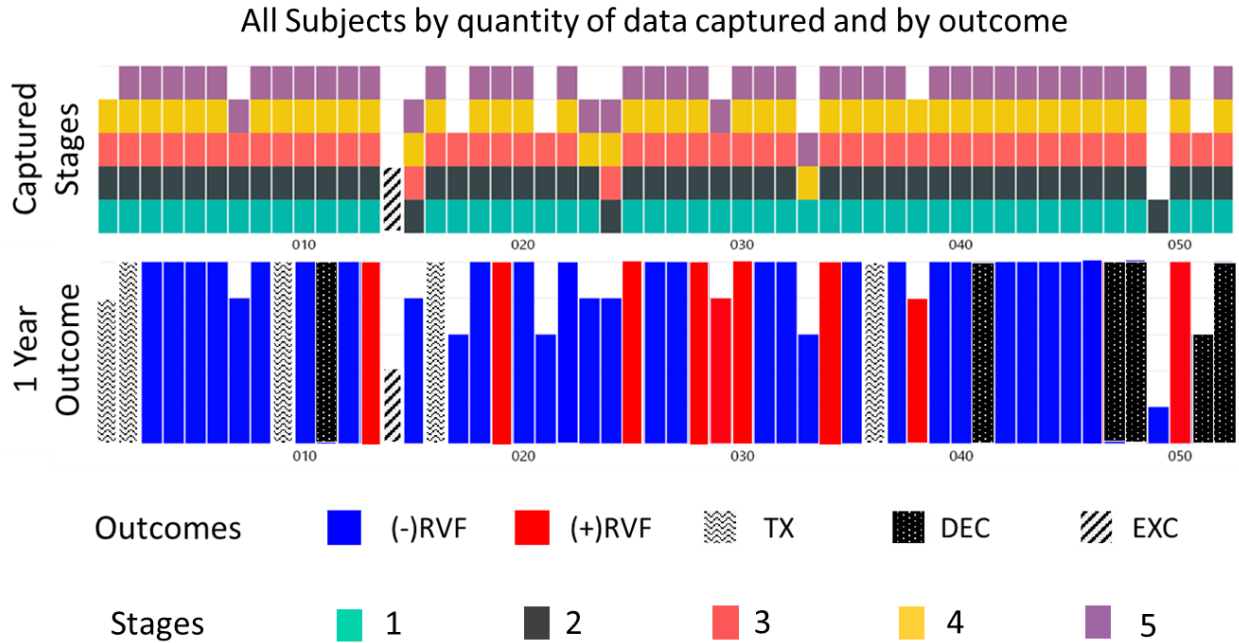


Figure 14-(Top) Visual representation of pressure data acquired per patient by stage. (Bottom) pressure data acquired per patient by outcome. Abbreviations: (-)RVF = no RV failure, (+)RVF = RV Failure, TX = transplant before one year, DEC = deceased before one year, EXC = excluded from study per surgeon request. Although only 51 subjects were included in the cohort, 52 studies were observed. At the request of the surgeon a subject was excluded from the study.

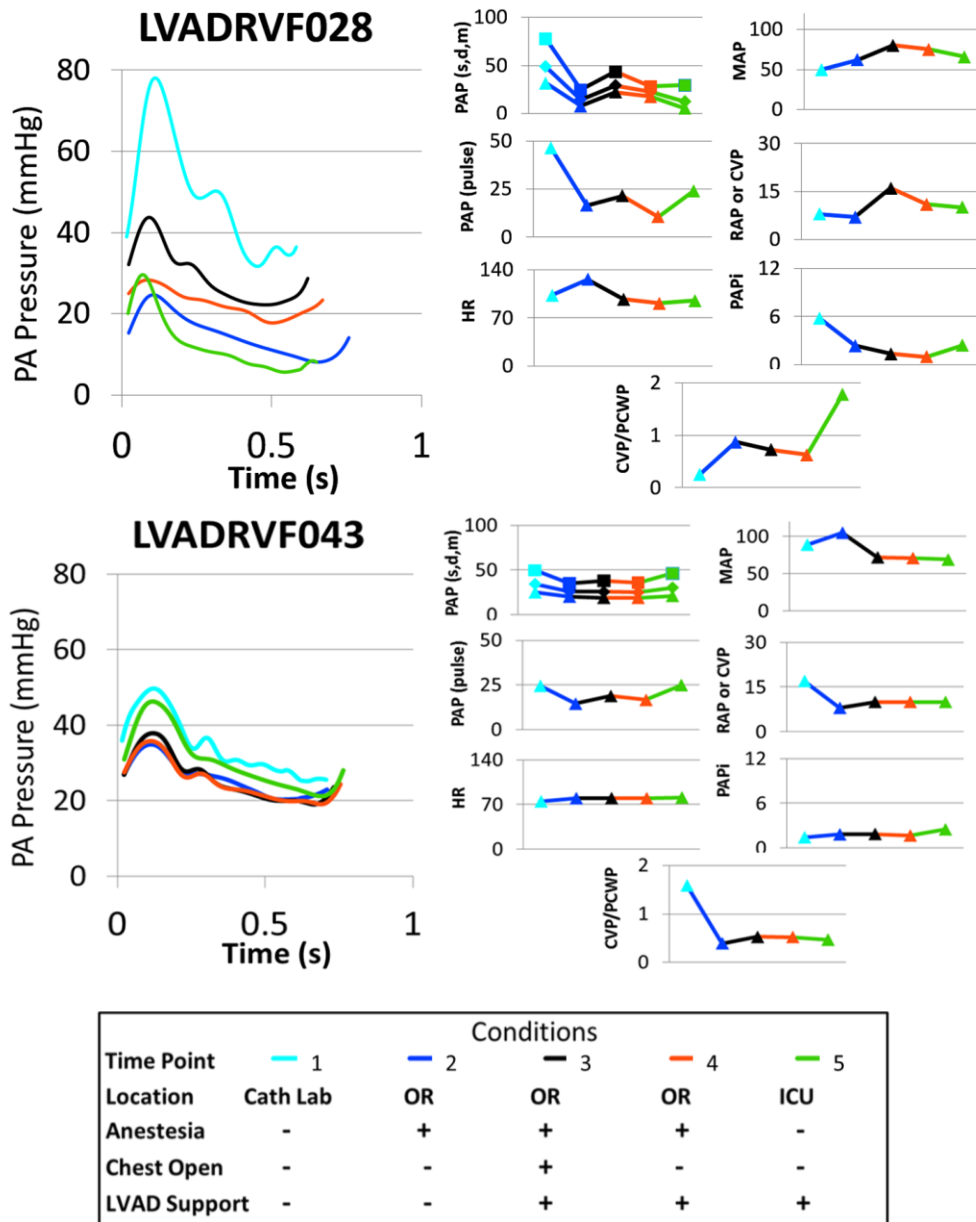
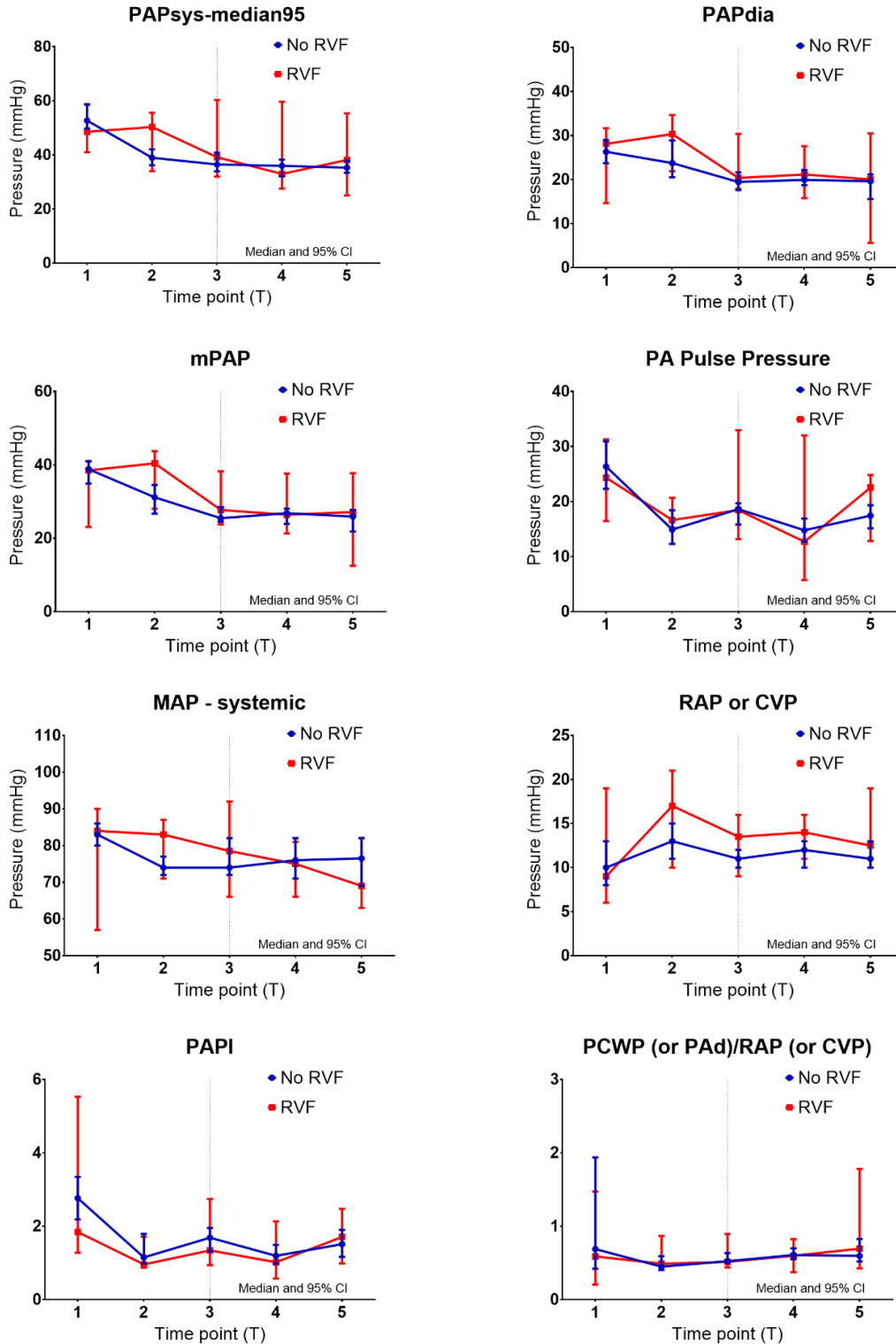


Figure 15- (Left) Average representative beats (ARBs) for each timepoint. (Right) Parameters derived by from each ARB at each timepoint. (Bottom) Conditions for each timepoint. (Abbreviations: PA= Pulmonary Artery, PAP = PA pressure (mmHg), s = systolic, d = diastolic, m = mean, HR= heart rate (beats/min), MAP = Mean Aortic Pressure (systemic, mmHg), RAP = right atrial pressure (mmHg), CVP= central venous pressure (mmHg), PCWP = pulmonary capillary wedge pressure (mmHg), PAPI = PA pulsatility index.



**Figure 16- Pressure-derived parameters in the time domain versus timepoint (T) for subjects with RVF (Red) and without RVF (Blue). Vertical line at T(3) indicates timepoint of LVAD implant. (Abbreviations: RVF = right ventricular failure; PA= Pulmonary Artery, PAP = PA pressure (mmHg), sys = systolic, dia = diastolic,**

**m = mean, MAP = Mean Aortic Pressure (systemic, mmHg), RAP = right atrial pressure (mmHg), CVP= central venous pressure (mmHg), PCWP = pulmonary capillary wedge pressure (mmHg), PAPI = PA pulsatility index.**

## **2.4 Assessment of RV Afterload in the Frequency Domain using Pulmonary Vascular Impedance**

### **2.4.1 Description**

Pulsed-wave Doppler velocity signals were recorded when possible to calculate PVZ in the frequency domain. Because standard surgical protocol includes the removal of a TEE probe before chest closure, Doppler velocities were recorded for T(1), T(2), and T(3) only, and therefore only a subset of the data was used for calculation of PVZ. Using this smaller group of patients, afterload in the frequency domain was calculated to determine if there was a difference in PVZ between subjects with chronic RVF and those with no RVF.

### **2.4.2 Methods**

Single beats were selected for both PAQ and Harmonics ( $z$ ) of waves were calculated by Fast Fourier Transform (FFT) within MATLAB (MathWorks, Natick, MA, USA).  $PVZ(z)$  was calculated as  $FFT(P(t))/FFT(Q(t))$ . Total pulmonary resistance  $Z(0)$ ; characteristic impedance  $Z_c$ , mean of  $PVZ(2-4)$ ; and vascular stiffness ( $Z1+Z2$ ) were compared at T(1,2,3) between +/-RVF groups.

### **2.4.3 Statistical Methods**

Comparisons at each individual time point for each  $Z0$ ,  $Z_c$ , and  $Z1+Z2$ , were conducted using a Kruskal Wallis H-test. Rate of change for individual parameters between timepoints was

also attempted between timepoints T(2) and T(3). Results were deemed significant at  $p < 0.05$ . In the case of the study in the frequency domain, a mixed effects mixed effects model could not be attempted due to the lack of sufficient numbers in each group.

#### **2.4.4 Results**

Composition of the Doppler dataset is shown in Figure 17. PVZ was able to be calculated for at least one time point for 43 of 51 subjects, including 7 with RVF. Retrospective PVZs could be constructed for  $n = 38$  (6 with RVF). The number of prospective PVZs for T(2) and T(3) were lower (17 (5 with RVF) and 18 (5 with RVF), respectively) due to no Doppler or pressure signals taken, technically difficult echo studies, difficult catheter placement, or malfunctioning catheter. On the other hand, there was a far larger window of time in which retrospective pressure and Doppler could be obtained. An example of a subject with all 3 PVZ spectra calculated is shown in Figure 18.

Median time between PAQ and PAP at T1 was 2.7 days (range .02-60) and time to implant from last procedure was 3 days (range 1-37); median time between captures was .034 minutes (range .05-65) for T2 and T3. Figure 19 shows the difference in heartrates for each subjects' PAP and PAQ data at all timepoints. There was generally good agreement in HR between PAP and PAQ acquisitions. The largest difference was found in T1, likely due to wider range of time between data captures. The most extreme difference between heartrates occurred for one subject in T(2), due to arrhythmia.

Figure 21 shows the mean and 95% confidence interval for all spectra for each group at each timepoint and parameter. General trends of decreasing Z0 and ZC, can be seen with all subjects combined, as one might expected due to optimization of patient hemodynamics

immediately prior to implant, followed by unloading due to the actual LVAD. However, it is also apparent that there is much overlap between outcome groups and large confidence intervals. A significant difference could only be found at T(1) for Z(1)+Z(2) with the full set of subjects. Data were then limited to captures that had a time difference of less than 96 hrs (see Figure 20), both between captures and from latest capture to surgery. The difference between groups was no longer significant when a time limit was imposed.

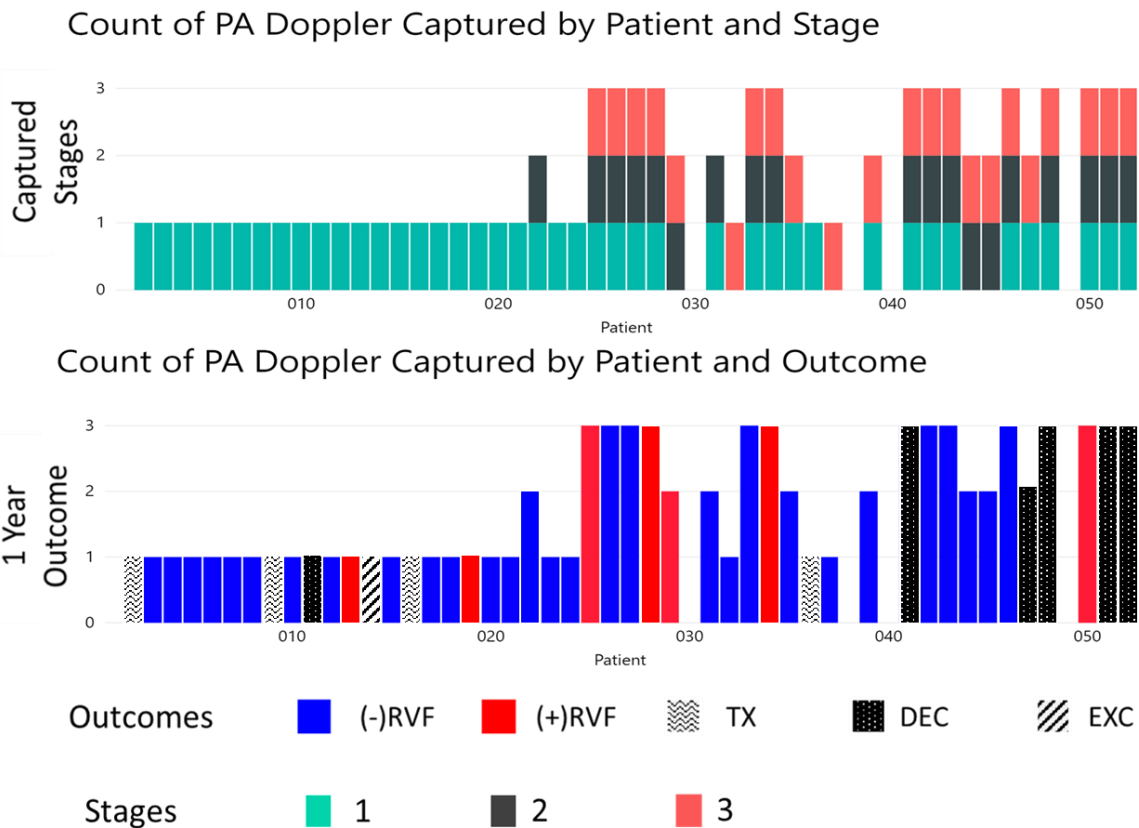


**Figure 17- Count of PA Doppler signals by stage and by outcome. These waveforms, compined with pressure waveforms from previous section were used to calculat PVZ. Abbreviations: (-)RVF = no RV failure, (+)RVF = RV Failure, TX = transplant before one year, DEC = deceased before one year, EXC = excluded from study per surgeon request. Although only 51 subjects were included in the cohort, 52 studies were observed. At the request of the surgeon a subject was excluded from the study.**

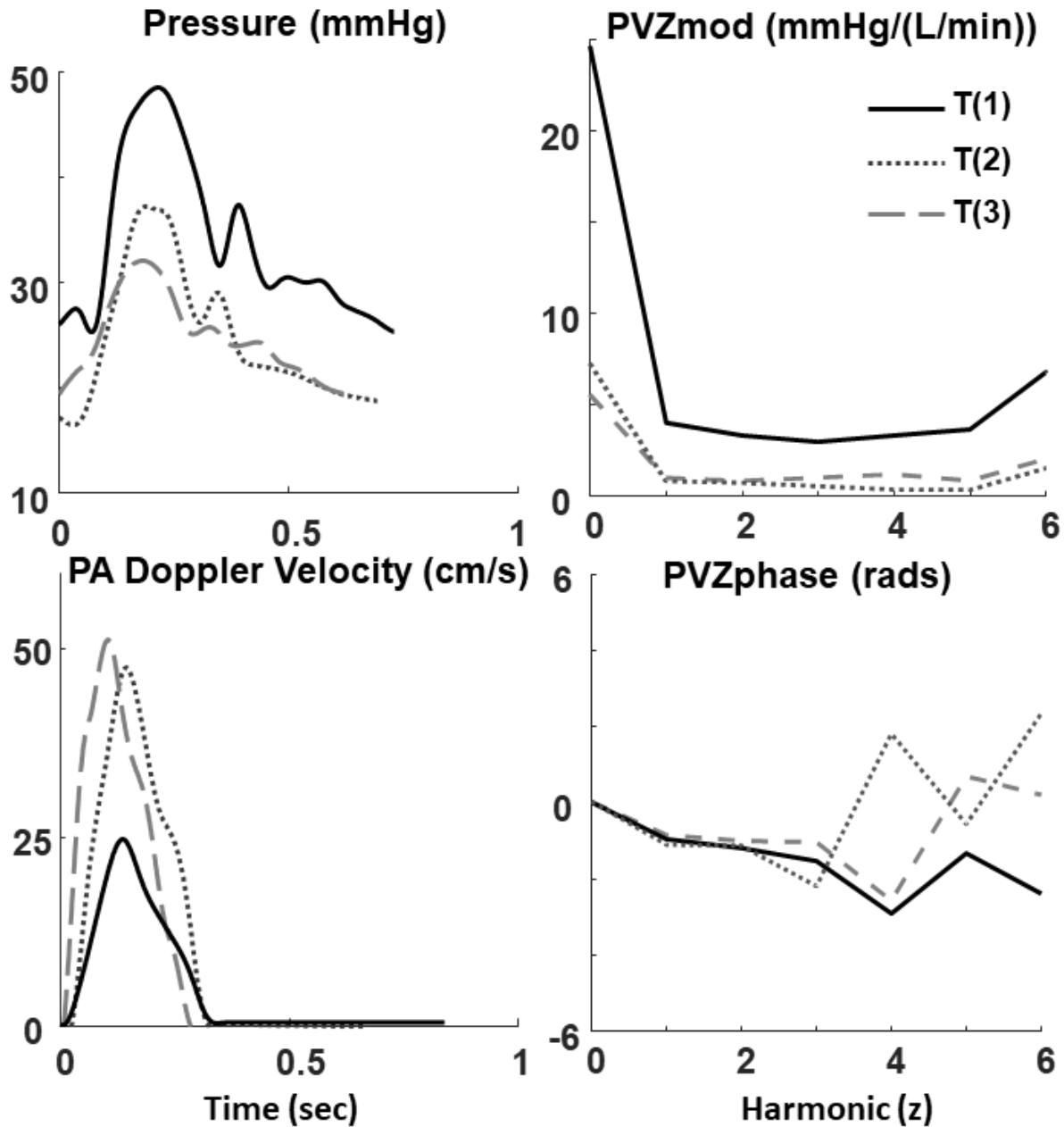
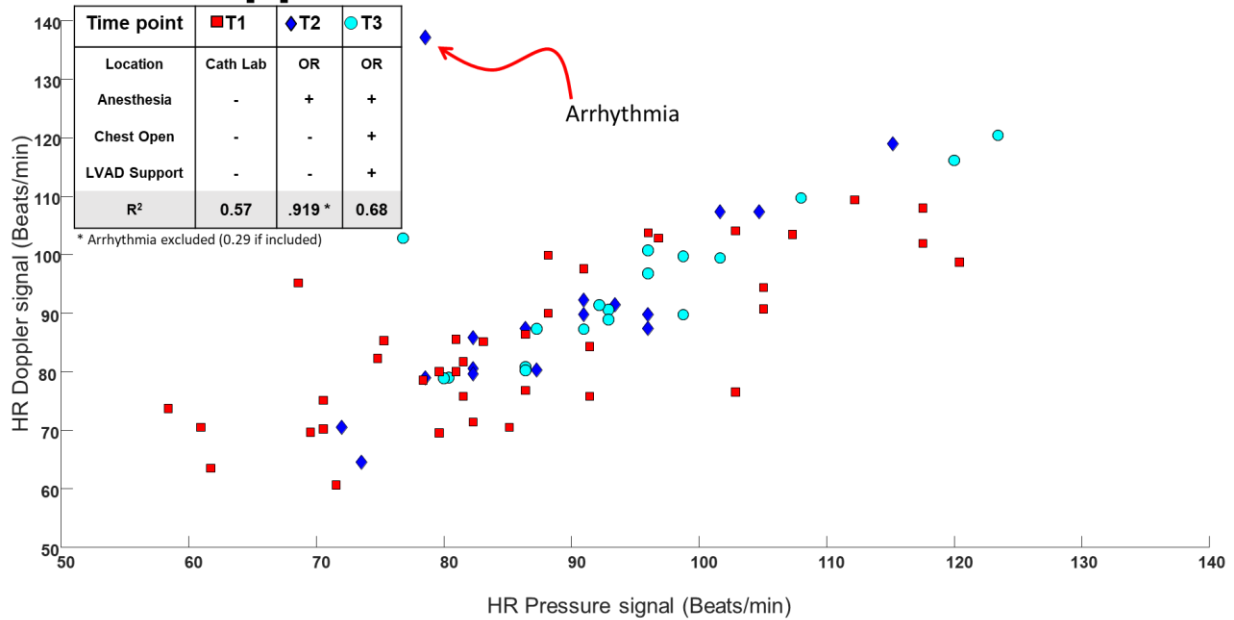


Figure 18- Components used for calculation of pulmonary vascular impedance (PVZ) and the resulting spectra from a single subject at all three timepoints. (Top left) Average representative beats for pressure. (Bottom left) Average representative beats for pulsed-wave Doppler velocity. (Top right) Modulus of the impedance spectrum. (Bottom right) Phase difference at each harmonic. Abbreviations: mmHg = millimeters of mercury, mod= modulus, L/min = liters per minute, sec = seconds, cm/s = centimeters/second, rads = radians.

# Doppler Heart Rate vs RHC Heart Rate



**Figure 19- Heart rate comparisons for PVZ at all 3 timepoints. One subject at T(2) had an arrhythmia which caused the largest individual difference in heart rate. As a group, T(1) had the heart rate differences, likely due to time elapsed between captures of Doppler Velocity and RHC. Abbreviations: HR = heart rate; RHC = right heart catheterization.**

## T(1) Time between studies vs time to implant

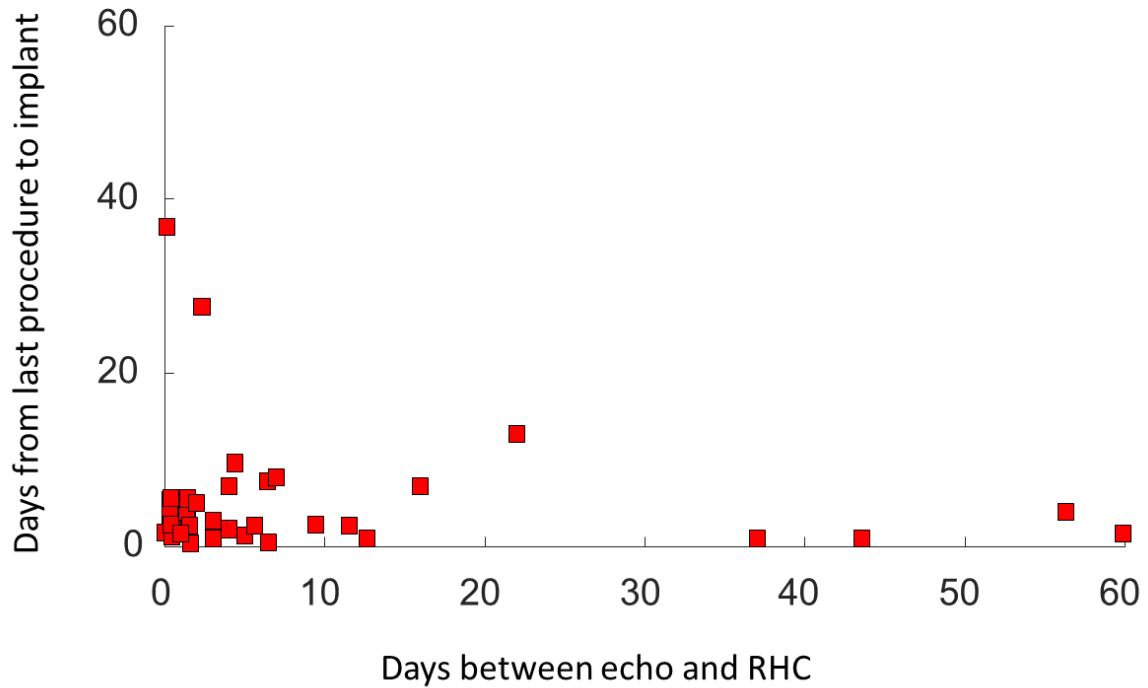


**Figure 20-Shortest time to surgery for T(1) vs time between procedures (echocardiography and right heart catheterization for T(1)). Large periods of time may have elapsed between subjects' echo and right heart catheterization, or between last study and implant. Comparison of PVZ by 1-year outcome was later limited to a maximum of 96 hours between captures, and 96 hours between last capture and surgery in order to decrease likelihood of error. PVZ = pulmonary vascular impedance, RHC = right heart catheterization.**

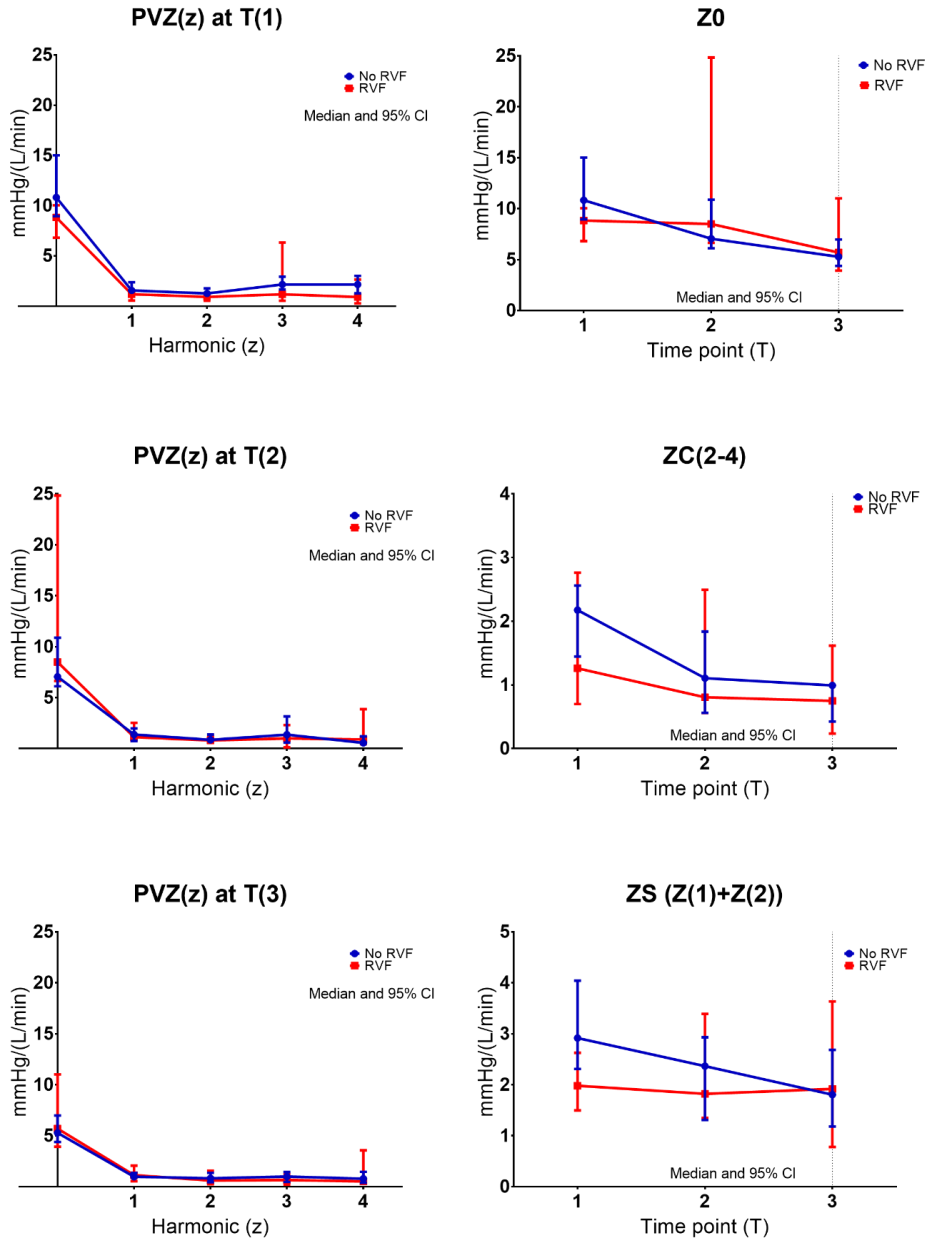


Figure 21- PVZ spectra and calculated parameter results for subjects with and without RVF (red, and blue, respectively). Dotted line indicates timepoint of device implant. A significant difference could only be found at T(1) for PVS when using the full set of subjects. However, once data were limited to captures that had a time difference of less than 96 hrs (see Figure 20), both between captures and from latest capture to surgery, the data were no longer significant. Abbreviations: RVF = right ventricular failure. PVZ(z) = pulmonary vascular impedance versus harmonic (z), ZS = stiffness, ZC = characteristic impedance, Z0 = total pulmonary resistance (steady component), CI = confidence interval.

## 2.5 Discussion

Total afterload faced by the RV was successfully calculated via composite PVZ using only asynchronous standard of care pulsed-wave Doppler velocity and PA pressure. The waveforms were re-digitized and decomposed in the frequency domain via FFT, with PVZ calculated as  $PVZ(z) = P(z)/Q(z)$ . The shape of the impedance spectra resembles that which are generated via simultaneous recording of pressure and flow. It is difficult to determine accuracy of the PVZ values because simultaneous acquisition has not yet been performed in LVAD subjects. Also, since single beats were selected for PVZ (due to limitations with code), the results were more susceptible to high-frequency noise. If PCWP were known for all timepoints and subtracted from mean PA pressure, Z0 values would be lower because they would reflect PVR as opposed to TPR. The resulting PVZ spectra were grouped by RVF outcome out to one year. When grouped by RVF outcome out to one year, no difference in PVZ was found.

Limitations in this study include small sample sizes, especially when calculating parameters in the frequency domain resulted in limited statistical testing. Time between captures in T(1) is likely a significant source of error. This is because pulmonary vascular impedance requires the assumption that the pulmonary vasculature is a linear time-invariant system. Many changes in hemodynamic state can change over several days, while short periods of time in between pressure and Doppler captures like those taken within the same timepoint in the OR are negligible. Also, if a change did occur due to speed change of the pump or medication dosage change during implant, a new capture would be recorded after steady-state was reached. This could not be done for retrospective captures.

While this work proved feasibility of PVZ assessment and provided pilot data, it would benefit from a structured prospective protocol with defined time limits for captures and a larger

sample size. If this study were replicated in a larger cohort of patients, and the findings were confirmed, it would mean that future studies should focus on other components of the RV and pulmonary circulation at large, specifically function and coupling.

With that said, it should be noted that after completion of this work, the definitions for RV failure have changed. Kormos et al recently re-defined RV failure in order to facilitate more standardized clinical research involving mechanical circulatory support, including giving long-term RVF its own designation.[58] Any re-analysis of this data or proposal of a larger study will need to use the new definitions moving forward.

## **3.0 Facilitation of Rapid Assessment of Pulmonary Vascular Impedance in the Clinical Setting**

### **3.1 Description**

Overload of the right ventricle (RV) frequently leads to heart failure and death. Therefore, characterizing the full afterload encountered by the RV is critical. The pulmonary vascular impedance (PVZ) spectrum, graphed in the frequency domain, is the only way to fully characterize the combined steady and pulsatile afterload faced by the right ventricle (RV).[59, 60] Analysis of PVZ to characterize the ventricular afterload has been performed for many decades in the research setting.[11, 59, 61-66] Unfortunately, current technical and cost limitations allow only the steady component (pulmonary vascular resistance (PVR) or total pulmonary resistance (TPR)) to be reported clinically.

In Chapter 2.0 screen captures of pressure and Doppler velocity signals were redigitized by meticulously adding waypoints to an entire capture. Only then could the data be exported to a separate program for analysis, and another for compiling and reporting. So, while the earlier work has successfully shown that PVZ can be calculated using standard of care data, it was neither rapid nor intuitive. Both qualities are necessary for PVZ to become commonplace in the clinic and in clinical research. The solution is to create a graphical, stand-alone program that uses clinically available asynchronous pressure and Doppler velocity captures to calculate, display, and compile the PVZ spectra and its resulting parameters for clinicians and researchers.

### 3.2 Methods

MATLAB-based software, called CompositePVZ©, was designed to analyze a patient's afterload and its changes during a study. This required 3 items: 1) A parasternal short axis screen capture at the base of the heart from TTE or TEE for measuring diameter, (alternatively a known diameter value previously measured can be used as a substitute), 2) screen capture of PA pulsed-wave Doppler velocity signal in the proximal PA from either TTE or TEE with ECG signal and 3) PA pressure signal with ECG signal obtained during standard right-heart catheterization. All of these can be obtained from standard RHC and Echo reports found in electronic health records (EHR).

Each capture imported into the software is then be calibrated using scales commonly found on images. The diameter is measured (see

Figure 22), and CSA is calculated by multiplying the diameter squared by  $\pi/4$ . Redigitization of the pressure waveforms is performed by selecting a region that contains multiple beats from the signal of interest. Once selected an automated border detection routine implements a time-frequency analysis function, called "tfridge" [67], within MATLAB that detects the signal, and traces it. The routine then overlays the signal on top of the image for inspection. The same task is then performed over the region containing the ECG signal in the same screen capture. Once completed for pressure, the process is repeated for pulsed-wave Doppler velocity and its ECG signal. Due to the low signal to noise ratio encountered with Doppler, manual editing of the traced Doppler signal may be performed by the user. An example of the traced signals for pressure and velocity is shown in Figure 23.

Following re-digitization, the function resamples the waveforms at 1000 Hz. The product of  $V(t)$  and CSA is calculated to obtain flow ( $Q(t)$ ). Mild noise reduction is performed via a

Savitzky-Golay filtering.[68] Individual beats separated by R-R interval via the ECG signal are selected to generate individual beats for both  $P(t)$  and  $Q(t)$ . The R-waves of the QRS signal are detected using a Pan Tompkins- based routine that was obtained as open-source code from MATLAB Central file exchange (See

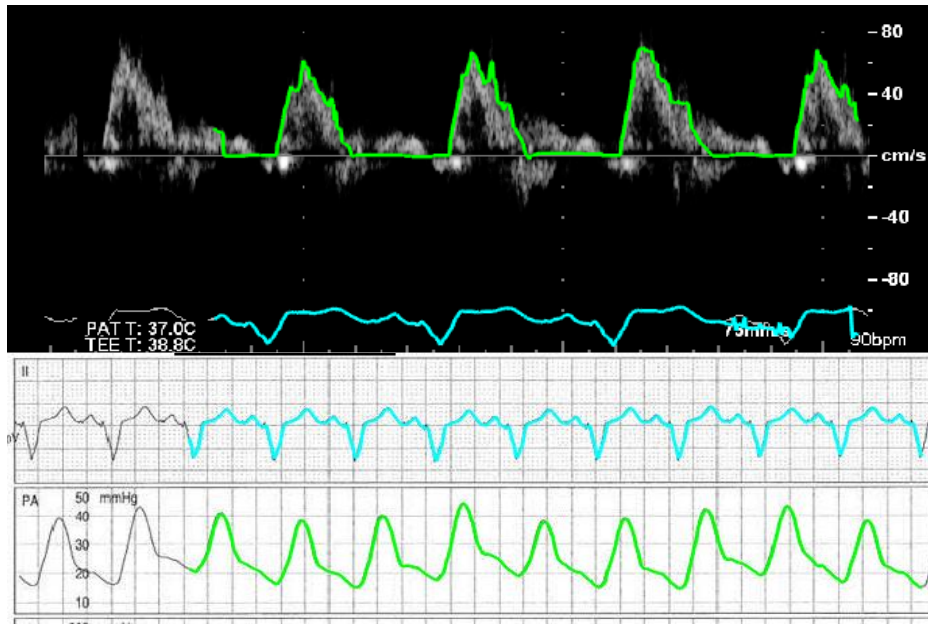
Figure 24). [69, 70] The individual beats are stacked on one another and are either selected or de-selected in order to generate an ARB.

The ARBs are then decomposed into harmonics ( $z$ ) via FFT, describing  $P(z)$  and  $Q(z)$  in the frequency domain. Modulus, calculated as the ratio of  $P(z)$  to  $Q(z)$  are plotted versus harmonics  $z(n)$  along with the phase difference between the two signals (see

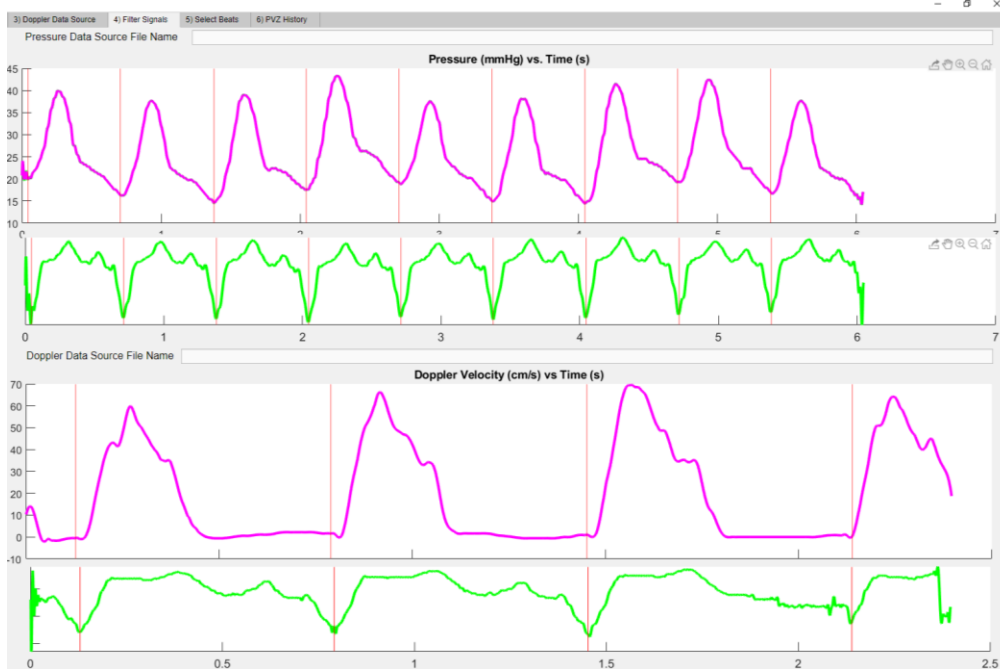
Figure 25).  $Z(0)$  is the mean value of the signal,  $z(1)$  is equal to the fundamental frequency (reported in Hz as the inverse of heart rate), and higher harmonics  $z(2)$  through  $z(N)$  which are multiples of  $z(1)$ .  $N$  is the maximum frequency from which PVZ can be determined by the fidelity of the catheter signals.



Figure 22- Parasternal short axis view of the heart using 2-dimensional ultrasound. Two measurements are made: The measurement on the left is for calibration purposes, and the measurement on the right is measuring the diameter of the pulmonary artery.



**Figure 23- (Top) Automated border detection of pulmonary arterial pulsed-wave Doppler velocity with electrocardiogram. Interference in the signal overlay can be observed at the end of the ECG signal. (Bottom) automated border detection from pulmonary arterial pressure waveform obtained via fluid-filled Swann Ganz catheter and electrocardiogram.**



**Figure 24- Tracings of Doppler velocity and pressure waveforms separated into individual beats via R-wave detection.**

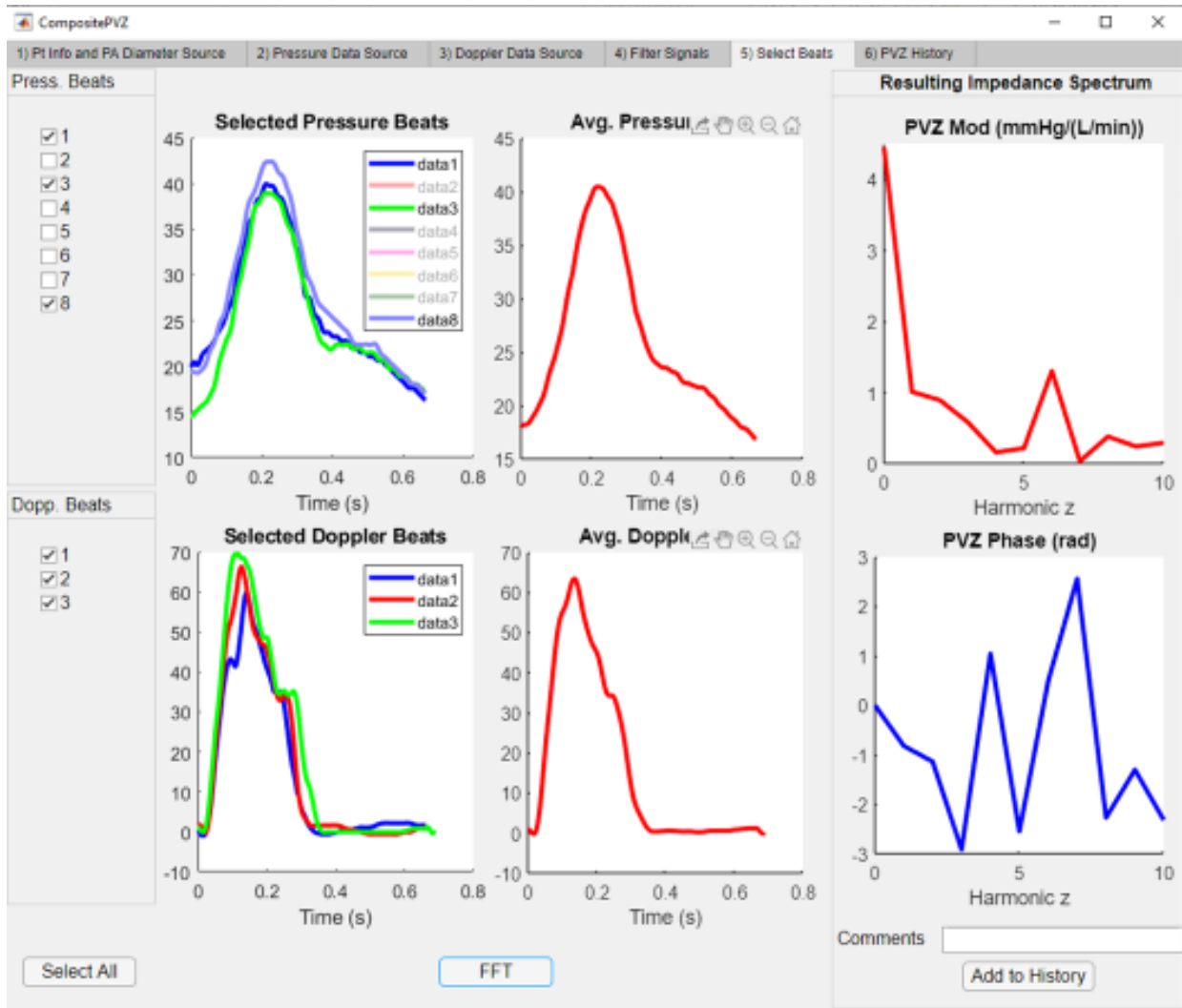


Figure 25- (Left) selection of individual beats for generation of average representative beats (middle). The average representative beats decomposed into wavelets via Fast Fourier Transform to calculate Magnitude (Top Right) and phase (bottom) of pulmonary vascular impedance.

### 3.3 Results

Figure 26 shows the resulting overlay of PVZ at two timepoints of a study involving the same subject under different conditions. Additional parameters that are calculated include:  $Z_0$ ,  $Z_c$  and stiffness ( $Z_1+Z_2$ ), cardiac output, power, and location of the first minima. The investigator can acquire multiple captures and choose which to include and exclude. The workflow is similar to cardiac output calculations in the catheterization lab. Parameters from selected spectra are then plotted and can be exported as a table for further analysis. A full display of the graphical user interface and all steps for analysis is featured in Appendix A, and a video of the software in use has been submitted along with this document ([Video 1](#)).

Signal interference provided some difficulty with beat separation and analysis. Interference was most often observed when overlap of text and ECG occurred, obscuring an R-wave. Other issues that were problematic included ECG noise or arrhythmia. This occurred most frequently with pulsed-wave Doppler waveforms due to the layout of the image, the low signal to noise ratio, and the number of beats that were included in the image. An example of overlay interference can be seen towards the end of the Doppler ECG in Figure 23. Despite this, corrections to the image prior to importation, such as erasing text or tick marks in an image editing program, improved R-wave recognition.



**Figure 26-** (Top Left) Multiple impedance spectra can be calculated and overlaid from the same capture to show changes due to beat selection. Additionally, spectra can be calculated for multiple timepoints to observe changes during a protocol. (Bottom Left) The end user has the ability to select which spectra to keep and which to hide by checking the “Include” boxes for spectra of choice. (Right) Time series for the resulting parameters from both time and frequency domain are plotted for the selected spectra.

### **3.4 Discussion**

A graphically driven analysis of PVZ, calculated from standard of care right heart catheterization and echocardiography is possible. A system such as this can enable clinicians to rapidly assess the afterload faced by a patient's RV. However, due to the asynchronous manner in which the data is obtained, care should be taken to minimize time between TTE or TEE and right heart catheterization and to ensure that heart rates and rhythms are similar to avoid error. If these limitations can be avoided, multiple clinical applications exist, including drug studies, exercise studies, and evaluations of surgical interventions that alter afterload.

Future versions of the software will include ways to manually edit overlay interference within the program, such as blocking out regions where text or tick marks which may cause the tracing to deviate from the actual signal. Selection of filtering technique and filter strength will also need to be made adjustable. One final feature is a standardized report generator to go along with the excel spreadsheet that is exported at the end of a study and can be added to a subject's health records.

## 4.0 Conclusions and Future Directions

LVAD recipients who suffer from RVF post implant experience decreases in survival to transplant or continued support and increases in hospital stay. While many investigators have studied RVF in the acute and short-term, few have studied potential causes for chronic RVF. The work contained herein attempted to characterize the total afterload faced by the RV using PVZ calculated from standard of care procedures. Specifically, pulsed-wave Doppler velocity and PA pressure waveforms obtained pre- and perioperatively were recorded at timepoints of known hemodynamic change during implant. The waveforms were re-digitized and decomposed in the frequency domain via FFT, with PVZ calculated as  $PVZ(z) = P(z)/Q(z)$ . The resulting PVZ spectra were grouped by RVF outcome out to one year. No difference was found between groups.

Finding no difference in pre- and perioperative PVZ in LVAD patients with RVF does not mean that this dissertation was unsuccessful. Rather, it gives future direction for investigators. RV function, afterload, and coupling are all important facets of pulmonary circulation. If this study were replicated in a larger cohort of patients, and the findings were confirmed, it would mean that future studies should focus on coupling and function. Such studies would require the use of more advanced imaging techniques and measurement of pressure-volume loops, both require scarce resources and further justification for use.

In the past, calculation of PVZ would fall into the same category requiring high-fidelity micromanometry acquired simultaneous to echo. However, in addition to possibly ruling out perioperative afterload as a cause for chronic RVF, this work has shown that PVZ can be calculated in a manner that requires only data that already exists from standard of care echo and RHC. In the initial study, the re-digitization and calculation of PVZ with this data was labor intensive and

required several tools to complete the analysis. However, after learning from this initial technique, a new system was developed that can complete the same analysis using the same EHR but in a single graphically driven software package that resembles the workflow of RHC systems found in the clinical setting.

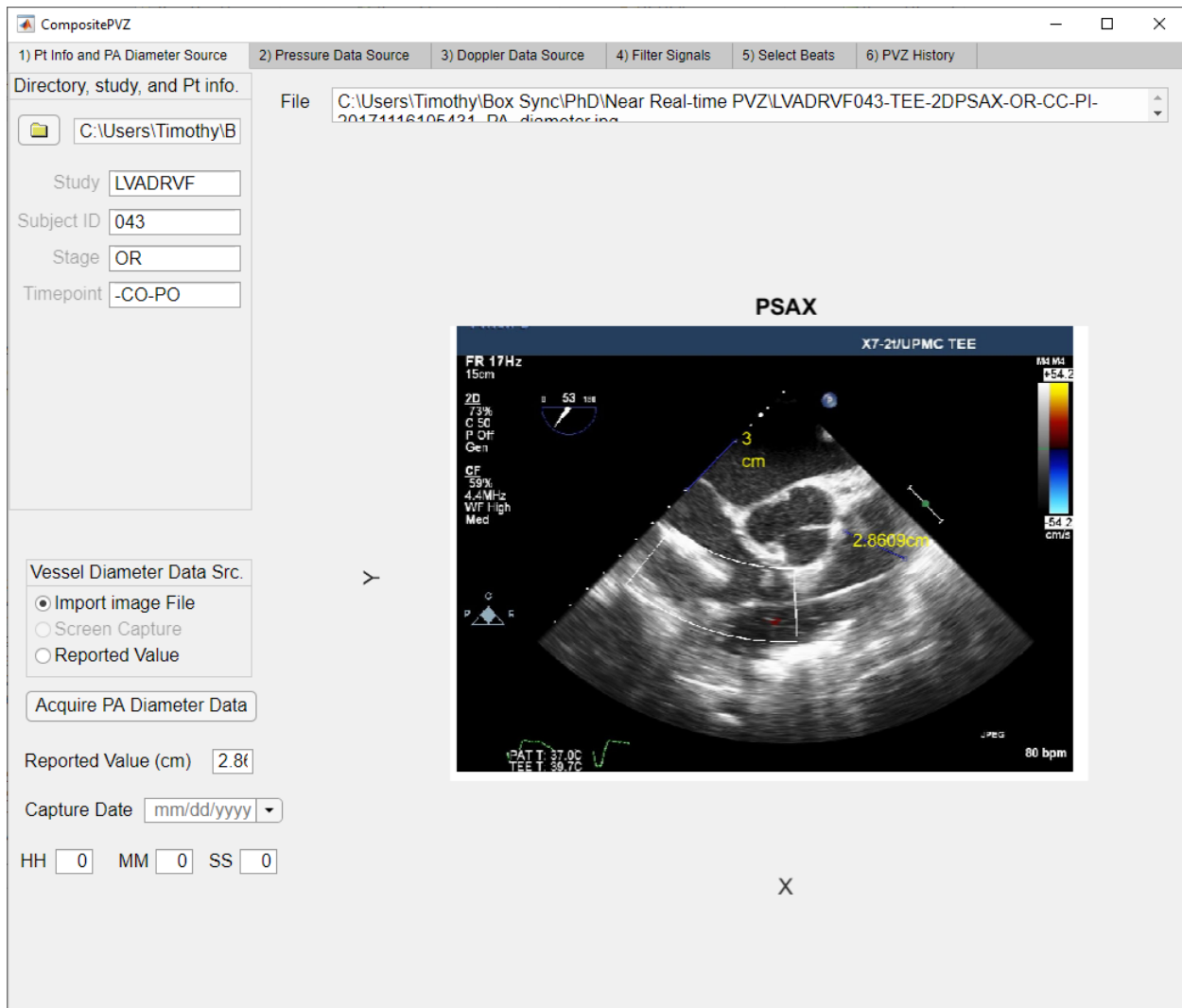
The use of CompositePVZ© is not limited to the analysis of data from a single patient suffering from Class IV HFrEF who received an LVAD. It can also potentially assist in determining the efficacy of other treatments that are thought to affect the RV afterload. For instance, members of the lab in which this dissertation was completed have previously studied novel drug treatments for WHO functional class II and III patients suffering from PH-HFpEF. In one such study PVZ was calculated in 14 subjects from a single center using simultaneously recorded pressure and Doppler velocity waveforms captured before and after inhalation of sodium nitrite. It was found that inhaled sodium nitrite decreased  $Z_c$  in subjects and increased RV efficiency and work. [71] While this was a subset of a single-center early Phase IIa safety and efficacy trial, the simplification of asynchronous acquisition (with limitations on time between pressure and echo) and the ability to process simple screen captures creates the possibility of using the CompositePVZ© software for core analyses in larger-scale, multicenter trials.[72]

Further work, however, needs to be performed to determine the limitations of this system. The maximum period between echo and pressure captures needs to be determined. The maximum period may differ for use with individual clinical patients who are stable and resting, as opposed to studies where hemodynamic state changes occur rapidly, such as drug or exercise studies. Also, the method of PA pressure measurement needs to be considered. The maximum frequency used in calculations of impedance at higher harmonics (i.e.,  $Z_c$ ), will need to be standardized for fluid-filled catheters. Once the questions have been thoroughly examined, we may likely see PVZ used

more frequently in the clinical setting, specifically in catheterization labs that are part of centers specializing in pulmonary hypertension and resulting RV failure.

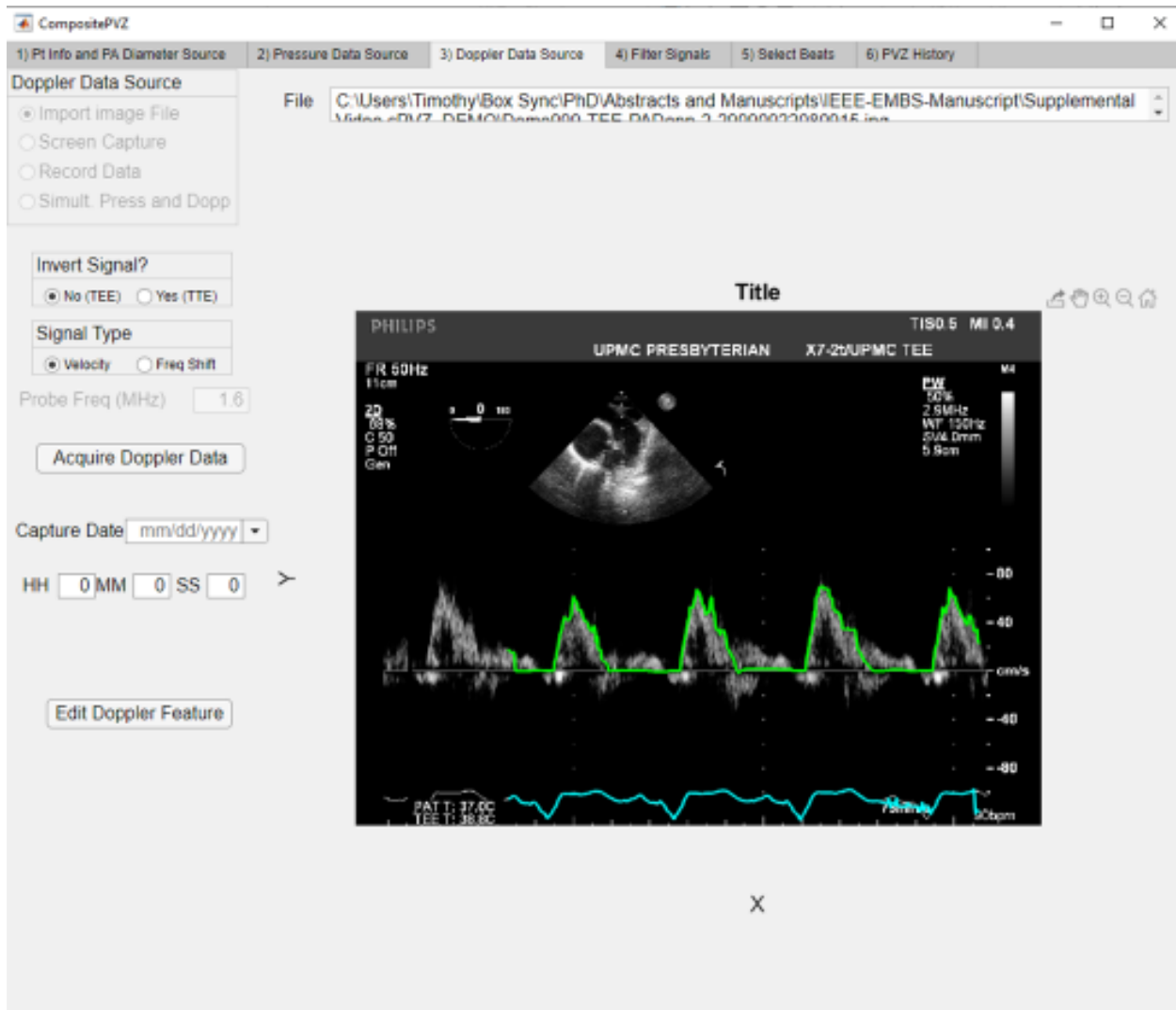
## Appendix A

Screen captures of full GUI layouts for all tabs in CompositePVZ© can be found in this section, beginning on the following page.

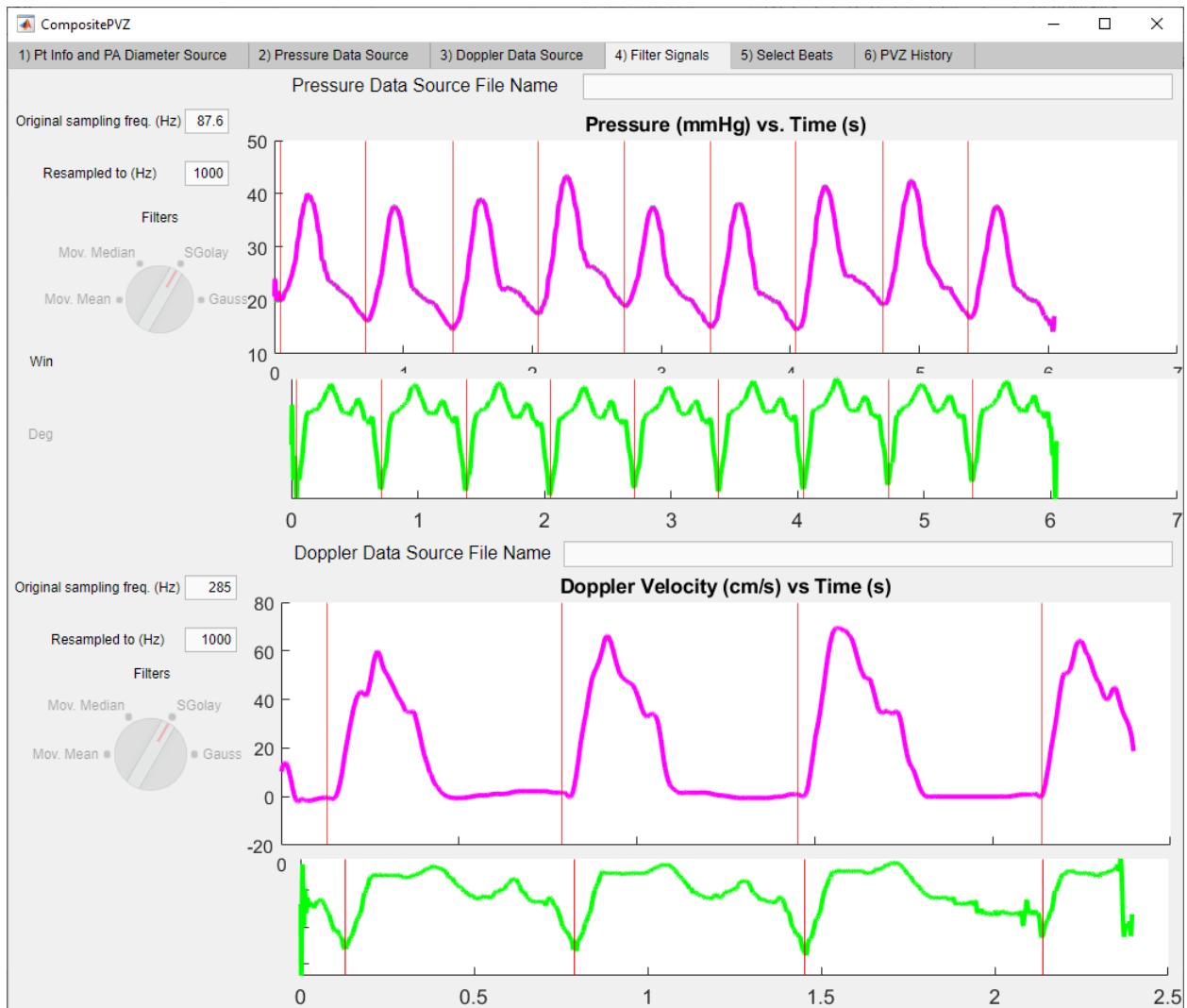


**Appendix Figure 1- Step 1: Input subject info and import parasternal short axis view at base of the heart (TTE or TEE). The image is calibrated using the image calibration key (the dots on the sector). Following calibration, the diameter of the PA is measured at the insertion sites of the PA valve leaflets.**

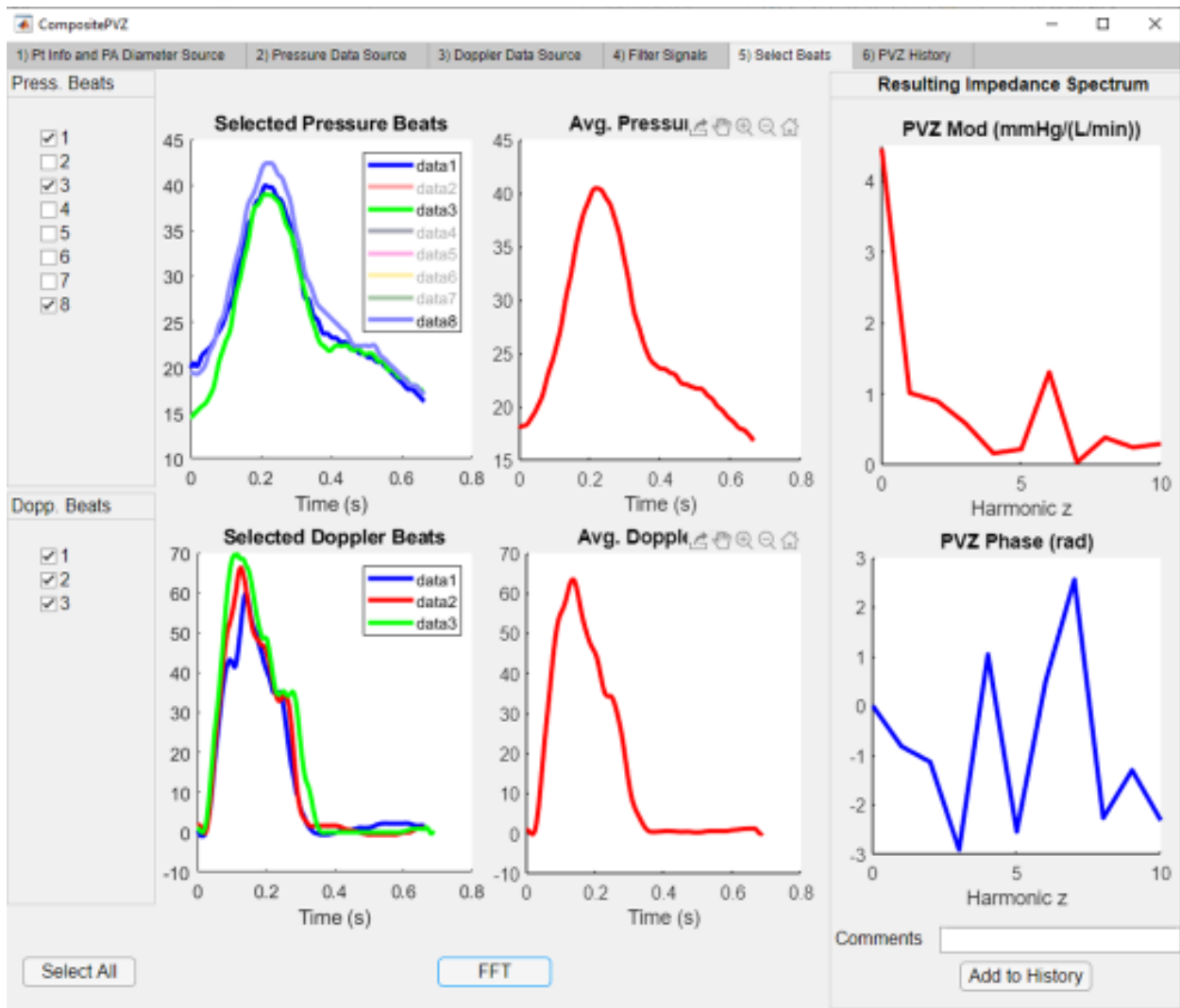




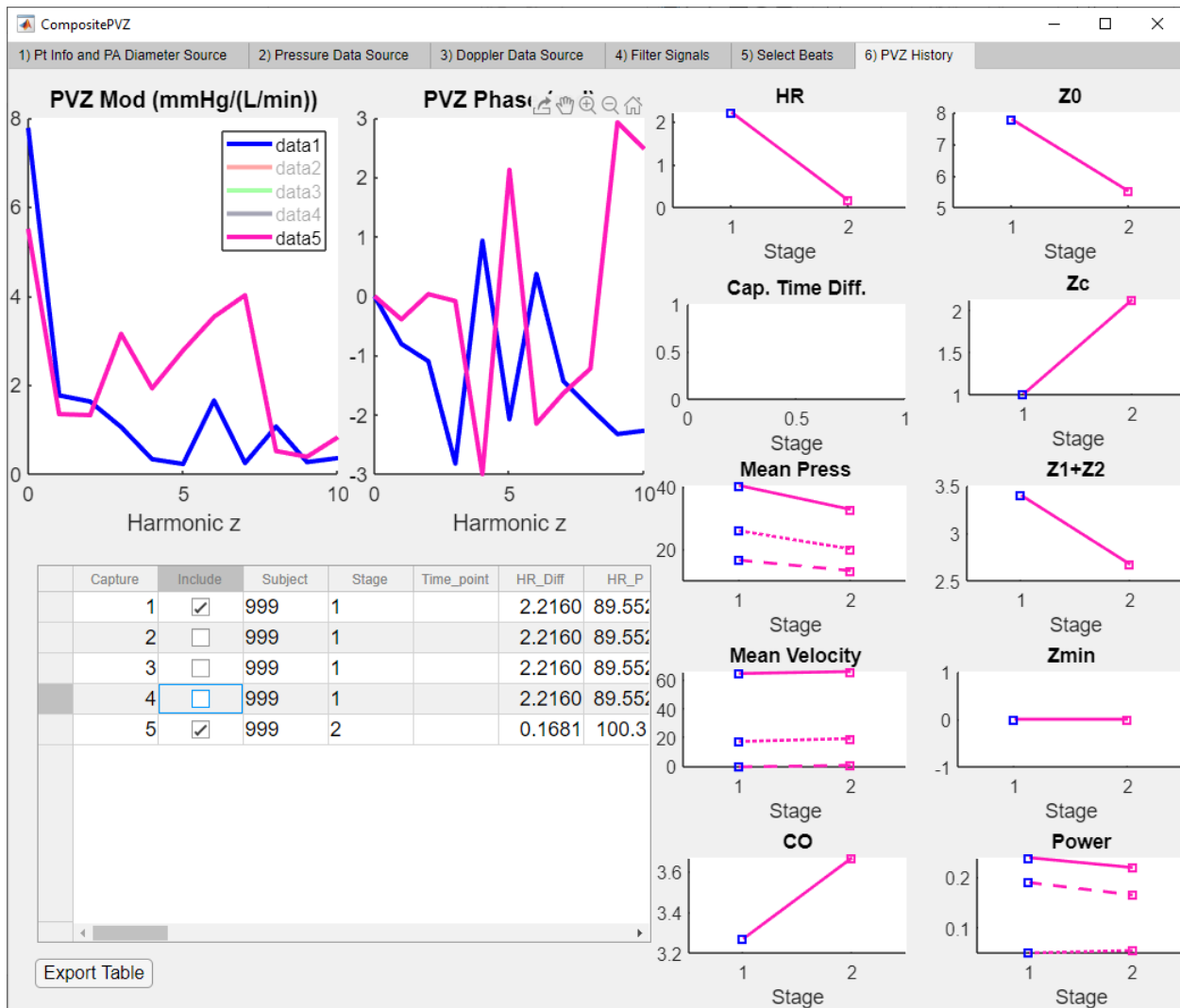
**Appendix Figure 3- Step3: The screen capture of PA pulswave Doppler signal is imported. This can be captured either via TTE or TEE. Values the image is calibrated by assigning values to the x-axis, y-axis, and origin. The user drags a boxes around the region containing the doppler and ECG waveforms. Automated border detection then traces and re-digitizes the selected signals. Due to low signal-to-noise ratio in Doppler signals, the user can make edits to remove any artifacts in Doppler tracing.**



**Appendix Figure 4- Step 4: individual beats are automatically identified using ECG signal to generate an R-R interval. If unsatisfactory, user can repeat steps 2 and/or 3 to improve signal fidelity.**



**Appendix Figure 5- Step 5: User selects pressure and velocity beats to form average representative beats in time domain and perform FFT to calculate a PVZ spectra. The user has the option of recording notes. Once satisfied with spectra, user saves it to PVZ History for comparison.**



**Appendix Figure 6- Step 6:** The user selects which PVZ spectra to compare graphically by checking or unchecking boxes in bottom left table. Spectra that are selected remain visible, and parameters derived from spectra are plotted in series on the right. All data (both selected and unselected) are exported in a .csv file once complete. The spreadsheet indicates which spectra were selected and deselected.

## Bibliography

1. Westerhof, N., *Snapshots of Hemodynamics An Aid for Clinical Research and Graduate Education*. 2. ed. 2010, Boston, MA: Springer US : Imprint: Springer.
2. Tedford, R.J., *Determinants of Right Ventricular Afterload (2013 Grover Conference Series)*. Pulmonary Circulation, 2014. **4**(2): p. 211-219.
3. Sagawa, K., et al., *Cardiac contraction and the pressure-volume relationship*, ed. K. Sagawa. 1988, New York: Oxford University Press.
4. Yancy Clyde, W., et al., *2013 ACCF/AHA Guideline for the Management of Heart Failure*. Circulation, 2013. **128**(16): p. e240-e327.
5. Virani, S.S., et al., *Heart Disease and Stroke Statistics&#x2014;2020 Update: A Report From the American Heart Association*. Circulation, 2020. **141**(9): p. e139-e596.
6. Westerdahl, D.E. and J.A. Kobashigawa, *Heart Transplantation for Advanced Heart Failure*. Cardiac Intensive Care, 2019: p. 504-524.e2.
7. Hahn, R.T., et al., *Guidelines for Performing a Comprehensive Transesophageal Echocardiographic Examination: Recommendations from the American Society of Echocardiography and the Society of Cardiovascular Anesthesiologists*. Journal of the American Society of Echocardiography, 2013. **26**(9): p. 921-964.
8. Greenspan, H., et al., *Doppler echocardiography flow-velocity image analysis for patients with atrial fibrillation*. Ultrasound in Medicine and Biology, 2005. **31**(8): p. 1031-1040.
9. Kubiak, G.M., et al., *Right Heart Catheterization-Background, Physiological Basics, and Clinical Implications*. Journal of clinical medicine, 2019. **8**(9): p. 1331.
10. A Milnor, W.R., A Conti, C. Richard, A Lewis, Kenneth B., A O'Rourke, Michael F., *Pulmonary arterial pulse wave velocity and impedance in man*. J Circulation research, 1969. **25**(6): p. 637-49.
11. Bergel, D.H. and W.R. Milnor, *Pulmonary Vascular Impedance in the Dog*. Circulation Research, 1965. **16**(5): p. 401-415.
12. Teuteberg, J.J., et al., *The Society of Thoracic Surgeons Intermacs 2019 Annual Report: The Changing Landscape of Devices and Indications*. Ann Thorac Surg, 2020. **109**(3): p. 649-660.

13. Bachman, T.N., *Development and Evaluation of the Quintessential Ventricular Cannula*, in *Bioengineering*. 2008, University of Pittsburgh.
14. Rose, E.A., et al., *Long-Term Use of a Left Ventricular Assist Device for End-Stage Heart Failure*. *New England Journal of Medicine*, 2001. **345**(20): p. 1435-1443.
15. Slaughter, M.S., et al., *Advanced Heart Failure Treated with Continuous-Flow Left Ventricular Assist Device*. *New England Journal of Medicine*, 2009. **361**(23): p. 2241-2251.
16. Rogers, J.G., et al., *Intrapericardial Left Ventricular Assist Device for Advanced Heart Failure*. *N Engl J Med*, 2017. **376**(5): p. 451-460.
17. Mehra, M.R., et al., *A Fully Magnetically Levitated Circulatory Pump for Advanced Heart Failure*. *N Engl J Med*, 2017. **376**(5): p. 440-450.
18. Olia, S.E., et al., *Mechanical blood trauma in assisted circulation: sublethal RBC damage preceding hemolysis*. *The International journal of artificial organs*, 2016. **39**(4): p. 150-159.
19. Lee, S.S., et al., *Strain hardening of red blood cells by accumulated cyclic supraphysiological stress*. *Artif Organs*, 2007. **31**(1): p. 80-6.
20. Zhao, R., et al., *Microscopic investigation of erythrocyte deformation dynamics*. *Biorheology*, 2006. **43**(6): p. 747-65.
21. Moazami, N., et al., *Axial and centrifugal continuous-flow rotary pumps: A translation from pump mechanics to clinical practice*. *The Journal of Heart and Lung Transplantation*, 2013. **32**(1): p. 1-11.
22. Antaki, J.F., et al., *Microhaemodynamics within the blade tip clearance of a centrifugal turbodynamic blood pump*. *Proceedings of the Institution of Mechanical Engineers, Part H: Journal of Engineering in Medicine*, 2008. **222**(4): p. 573-581.
23. Han, J.J., M.A. Acker, and P. Atluri, *Left Ventricular Assist Devices*. *Circulation*, 2018. **138**(24): p. 2841-2851.
24. Kirklin, J.K., et al., *Eighth annual INTERMACS report: Special focus on framing the impact of adverse events*. *J Heart Lung Transplant*, 2017. **36**(10): p. 1080-1086.
25. Shreenivas, S.S., J.E. Rame, and M. Jessup, *Mechanical circulatory support as a bridge to transplant or for destination therapy*. *Current heart failure reports*, 2010. **7**(4): p. 159-166.
26. Birks, E.J., et al., *Left Ventricular Assist Device and Drug Therapy for the Reversal of Heart Failure*. *New England Journal of Medicine*, 2006. **355**(18): p. 1873-1884.

27. Simon, M.A., et al., *Myocardial recovery using ventricular assist devices: prevalence, clinical characteristics, and outcomes*. *Circulation*, 2005. **112**(9 Suppl): p. I32-6.
28. Birks, E.J., et al., *Prospective Multicenter Study of Myocardial Recovery Using Left Ventricular Assist Devices (RESTAGE-HF [Remission from Stage D Heart Failure])*. *Circulation*, 2020. **142**(21): p. 2016-2028.
29. Flores, A.S., et al., *Echocardiographic assessment for ventricular assist device placement*. *Journal of thoracic disease*, 2015. **7**(12): p. 2139-2150.
30. Beyersdorf, F., J. Scheumann, and M. Siepe, *Implantation of the HeartMate 3—Description of the Surgical Technique*. *Operative Techniques in Thoracic and Cardiovascular Surgery*, 2017. **22**(3): p. 173-185.
31. Romano, M.A., J. Haft, and F.D. Pagani, *HeartWare HVAD: Principles and Techniques for Implantation*. *Operative Techniques in Thoracic and Cardiovascular Surgery*, 2013. **18**(3): p. 230-238.
32. Stulak, J.M., A. Abou El Ela, and F.D. Pagani, *Implantation of a Durable Left Ventricular Assist Device: How I Teach It*. *The Annals of Thoracic Surgery*, 2017. **103**(6): p. 1687-1692.
33. Castagna, F., et al., *The Unique Blood Pressures and Pulsatility of LVAD Patients: Current Challenges and Future Opportunities*. *Curr Hypertens Rep*, 2017. **19**(10): p. 85.
34. Bachman, T.N., et al., *In Vitro Evaluation of Ventricular Cannulation for Rotodynamic Cardiac Assist Devices*. *Cardiovascular Engineering and Technology*, 2011. **2**(3): p. 203-211.
35. Bhama, J.K., et al., *Development of an Ex Vivo Ovine Ventricular Assist Device Model for Intraventricular Visualization of the Inflow Cannula*. *The Journal of Heart and Lung Transplantation*, 2009. **28**(8): p. 860-861.
36. Ochiai, Y., et al., *Predictors of severe right ventricular failure after implantable left ventricular assist device insertion: analysis of 245 patients*. *Circulation*, 2002. **106**(12 Suppl 1): p. I198-202.
37. Kormos, R.L., et al., *Right ventricular failure in patients with the HeartMate II continuous-flow left ventricular assist device: Incidence, risk factors, and effect on outcomes*. *The Journal of Thoracic and Cardiovascular Surgery*, 2010. **139**(5): p. 1316-1324.
38. Patlolla, B., R. Beygui, and F. Haddad, *Right-ventricular failure following left ventricle assist device implantation*. *Curr Opin Cardiol*, 2013. **28**(2): p. 223-33.
39. Kapur, N.K., et al., *Mechanical Circulatory Support Devices for Acute Right Ventricular Failure*. *Circulation*, 2017. **136**(3): p. 314-326.

40. Wang, Y., et al., *Decision tree for adjuvant right ventricular support in patients receiving a left ventricular assist device*. The Journal of Heart and Lung Transplantation, 2012. **31**(2): p. 140-149.
41. Wang, Y., et al., *Prognosis of right ventricular failure in patients with left ventricular assist device based on decision tree with SMOTE*. IEEE Trans Inf Technol Biomed, 2012. **16**(3): p. 383-90.
42. Wang, Y., et al., *A Classification Approach for Risk Prognosis of Patients on Mechanical Ventricular Assistance*. Proc Int Conf Mach Learn Appl, 2010: p. 293-298.
43. Soliman, O.I., et al., *Derivation and Validation of a Novel Right-Sided Heart Failure Model After Implantation of Continuous Flow Left Ventricular Assist Devices: The EUROMACS (European Registry for Patients with Mechanical Circulatory Support) Right-Sided Heart Failure Risk Score*. Circulation, 2017.
44. Loghmanpour, N.A., et al., *A Bayesian Model to Predict Right Ventricular Failure Following Left Ventricular Assist Device Therapy*. JACC. Heart failure, 2016. **4**(9): p. 711-721.
45. Fitzpatrick Iii, J.R., et al., *Risk Score Derived from Pre-operative Data Analysis Predicts the Need for Biventricular Mechanical Circulatory Support*. The Journal of Heart and Lung Transplantation, 2008. **27**(12): p. 1286-1292.
46. Drakos, S.G., et al., *Risk Factors Predictive of Right Ventricular Failure After Left Ventricular Assist Device Implantation*. The American Journal of Cardiology, 2010. **105**(7): p. 1030-1035.
47. Atluri, P., et al., *Predicting Right Ventricular Failure in the Modern, Continuous Flow Left Ventricular Assist Device Era*. The Annals of thoracic surgery, 2013. **96**(3): p. 857-864.
48. Matthews, J.C., et al., *The Right Ventricular Failure Risk Score: A Pre-Operative Tool for Assessing the Risk of Right Ventricular Failure in Left Ventricular Assist Device Candidates*. Journal of the American College of Cardiology, 2008. **51**(22): p. 2163-2172.
49. Rich, J.D., et al., *The incidence, risk factors, and outcomes associated with late right-sided heart failure in patients supported with an axial-flow left ventricular assist device*. The Journal of Heart and Lung Transplantation, 2017. **36**(1): p. 50-58.
50. Kalogeropoulos, A.P., et al., *Validation of clinical scores for right ventricular failure prediction after implantation of continuous-flow left ventricular assist devices*. The Journal of Heart and Lung Transplantation, 2015. **34**(12): p. 1595-1603.
51. Tedford, R.J., et al., *PDE5A inhibitor treatment of persistent pulmonary hypertension after mechanical circulatory support*. Circ Heart Fail, 2008. **1**(4): p. 213-9.

52. Simon, M.A., *Assessment and treatment of right ventricular failure*. Nat Rev Cardiol, 2013. **10**(4): p. 204-18.
53. Committee, I.E. *INTERMACS Protocol 4.0, Appendix A- INTERMACS Adverse Event Definitions: Adult and Pediatric patients*. 5/15/2013; Available from: [http://www.uab.edu/medicine/intermacs/images/protocol\\_4.0/protocol\\_4.0\\_MoP/Appendix\\_A\\_INTERMACS\\_AE\\_Definitions\\_05152013.docx](http://www.uab.edu/medicine/intermacs/images/protocol_4.0/protocol_4.0_MoP/Appendix_A_INTERMACS_AE_Definitions_05152013.docx).
54. Bachman, T.N., et al., *A Novel Acquisition Technique to Utilize Swan-Ganz Catheter data as a Surrogate for High-fidelity Micromanometry within the Right Ventricle and Pulmonary Circuit*. Cardiovascular Engineering and Technology, 2013. **4**(2): p. 183-191.
55. Morine, K.J., et al., *The Pulmonary Artery Pulsatility Index is Associated with Right Ventricular Failure Following Left Ventricular Assist Device Surgery*. Journal of Cardiac Failure.
56. Kopman, E.A. and T.B. Ferguson, *Interaction of right and left ventricular filling pressures at the termination of cardiopulmonary bypass: Central venous pressure/pulmonary capillary wedge pressure ratio*. The Journal of Thoracic and Cardiovascular Surgery, 1985. **89**(5): p. 706-708.
57. Kiernan, M.S., et al., *Early Right Ventricular Assist Device Use in Patients Undergoing Continuous-Flow Left Ventricular Assist Device Implantation*. Incidence and Risk Factors From the Interagency Registry for Mechanically Assisted Circulatory Support, 2017. **10**(10).
58. Kormos, R.L., et al., *Updated definitions of adverse events for trials and registries of mechanical circulatory support: A consensus statement of the mechanical circulatory support academic research consortium*. The Journal of Heart and Lung Transplantation, 2020. **39**(8): p. 735-750.
59. Chesler, N.C., et al., *How to Measure Pulmonary Vascular and Right Ventricular Function*. Conference proceedings : ... Annual International Conference of the IEEE Engineering in Medicine and Biology Society. IEEE Engineering in Medicine and Biology Society. Conference, 2009. **2009**: p. 177-180.
60. Champion, H.C., E.D. Michelakis, and P.M. Hassoun, *Comprehensive invasive and noninvasive approach to the right ventricle-pulmonary circulation unit: state of the art and clinical and research implications*. Circulation, 2009. **120**(11): p. 992-1007.
61. Milnor, W.R., et al., *Pulmonary Arterial Pulse Wave Velocity and Impedance in Man*. Circulation Research, 1969. **25**(6): p. 637-649.
62. Grant, B.J.B. and B.B. Lieber, *Clinical significance of pulmonary arterial input impedance*. European Respiratory Journal, 1996. **9**(11): p. 2196-2199.

63. Chen, E.P., et al., *Nitric oxide improves pulmonary vascular impedance, transpulmonary efficiency, and left ventricular filling in chronic pulmonary hypertension*. The Journal of Thoracic and Cardiovascular Surgery, 1997. **113**(5): p. 849-857.
64. Brimiouille, S., *Effects of low flow on pulmonary vascular flow–pressure curves and pulmonary vascular impedance*. Cardiovascular Research, 1999. **42**(1): p. 183-192.
65. Huez, S., et al., *Feasibility of routine pulmonary arterial impedance measurements in pulmonary hypertension*. Chest, 2004. **125**(6): p. 2121-8.
66. Hunter, K.S., et al., *Pulmonary vascular input impedance is a combined measure of pulmonary vascular resistance and stiffness and predicts clinical outcomes better than pulmonary vascular resistance alone in pediatric patients with pulmonary hypertension*. American Heart Journal, 2008. **155**(1): p. 166-174.
67. MATLAB, *tfridge- Time-frequency ridges*, in *MATLAB Documentation*. 2019, MathWorks.
68. Schafer, R.W., *What Is a Savitzky-Golay Filter? [Lecture Notes]*. IEEE Signal Processing Magazine, 2011. **28**(4): p. 111-117.
69. Pan, J. and W.J. Tompkins, *A Real-Time QRS Detection Algorithm*. IEEE Transactions on Biomedical Engineering, 1985. **BME-32**(3): p. 230-236.
70. Sedghamiz, H., *Complete Pan Tompkins Implementation ECG QRS detector*. 2018: MATLAB Central File Exchange.
71. Bashline, M.J., et al., *The Effects of Inhaled Sodium Nitrite on Pulmonary Vascular Impedance in Patients With Pulmonary Hypertension Associated with Heart Failure With Preserved Ejection Fraction*. J Card Fail, 2020. **26**(8): p. 654-661.
72. Simon, M.A., et al., *Acute hemodynamic effects of inhaled sodium nitrite in pulmonary hypertension associated with heart failure with preserved ejection fraction*. JCI insight, 2016. **1**(18): p. e89620-e89620.